6 Hassanein AH, Mulliken JB, Fishman SJ *et al.* Evaluation of terminology for vascular anomalies in current literature. *Plast. Reconstr. Surg.* 2011; **127**: 347–8.
7 Al-Adnani M, Williams S, Rampling D *et al.* Histopathological reporting of pediatric cutaneous vascular anomalies in relation to proposed multidisciplinary classification system. *J. Clin. Pathol.* 2006; **59**: 1278–82.
8 Kollipara R, Odhav A, Rentas KE *et al.* Vascular anomalies in pediatric patients, updated classification, imaging, and therapy. *Radiol. Clin.* 2013; **51**: 659–72.
9 Nozaki T, Matumoto M, Mimura H *et al.* Imaging of vascular tumors with an emphasis on ISSVA classification. *Jpn J. Radiol.* 2013; **31**: 775–85.
10 Kuroda T, Kumagai M, Nosaka S, Nakazawa A, Takimoto T, Hoshino K. Critical infantile hepatic hemangioma: Results of a nationwide survey by the Japanese Infantile Hepatic Hemangioma Study Group. *J. Pediatr. Surg.* 2011; **46**: 2239–43.
11 Kulungowski AM, Alomari AI, Chawla A *et al.* Lessons from a liver hemangioma registry: Subtype classification. *J. Pediatr. Surg.* 2012; **47**: 165–70.
12 Mo JQ, Dimashkieh HH, Bove KE. GLUT1 endothelial reactivity distinguishes hepatic infantile hemangioma from congenital hepatic vascular malformation with associated capillary proliferation. *Hum. Pathol.* 2004; **35**: 200–9.
13 Lunetta P, Karikoski R, Penttila A *et al.* Sudden death associated with a multifocal type II hemangioendothelioma of the liver in a 3-month-old infant. *Am. J. Forensic Med. Pathol.* 2004; **25**: 511–14.
14 Taki M, Ohi C, Yamashita A *et al.* Successful treatment with vincristine of an infant with intractable Kasabach-Merritt syndrome. *Pediatr. Int.* 2006; **48**: 82–4.
15 Moore J, Lee M, Garzon M *et al.* Effective therapy of a vascular tumor of infancy with vincristine. *J. Pediatr. Surg.* 2001; **36**: 1273–6.
16 Hu B, Lachman R, Phillips J *et al.* Kasabach-Merritt syndrome associated kaposiform hemangio-endothelioma successfully treated with cyclophosphamide, vincristine, and actinomycin D. *J. Pediatr. Hematol. Oncol.* 1998; **20**: 567–9.
17 Fuchimoto Y, Morikawa N, Kuroda T *et al.* Vincristine, actinomycin D, cyclophosphamide chemotherapy resolves Kasabach-Merritt syndrome resistant to conventional therapies. *Pediatr. Int.* 2012; **54**: 285–7.
18 Leaute-Labreze C, Dumas de la Roque E, Hubiche T *et al.* Propranolol for severe hemangioma of infancy. *N. Engl. J. Med.* 2008; **358**: 2649–51.
19 Mazereeuw-Hautier J, Hoeger PH, Benlahrech S *et al.* Efficacy of propranolol in hepatic infantile hemangiomas with diffuse neonatal hemangiomatosis. *J. Pediatr.* 2010; **157**: 340–42.
20 Warmann S, Berram H, Kardorff R *et al.* Interventional treatment of infantile hepatic hemangioendothelioma. *J. Pediatr. Surg.* 2003; **38**: 1177–81.
21 Draper H, Diamond IR, Temple M *et al.* Multimodal management of endangering hepatic hemangioma: Impact on transplant avoidance: A descriptive case series. *J. Pediatr. Surg.* 2008; **43**: 120–26.
22 Rodriguez J, Becker N, O'Mahony C, Goss JA, Aloia TA. Long-term outcome following liver transplantation for hepatic hemangioendothelioma: The UNOS experience from 1987 to 2005. *J. Gastrointest. Surg.* 2008; **12**: 110–16.
23 Markiewicz-Kijewska M, Kapsrzyk W, Broniszczak D *et al.* Hemodynamic failure as an indication to urgent liver transplantation in infants with giant hepatic hemangiomas or vascular malformations; report of four cases. *Pediatr. Transplant.* 2009; **13**: 906–12.

© 2014 Japan Pediatric Society

症例報告

横紋筋肉腫治療後26年で発症した放射線誘発性軟骨肉腫の1例*

宇高　徹[*1)]　須佐美知郎[*1)]　中山ロバート[*1)]
渡部　逸央[*1)]　堀内　圭輔[*1)]　星野　健[*2)]
黒田　達夫[*2)]　佐々木　文[*3)]　向井万起男[*3)]
戸山　芳昭[*1)]　森岡　秀夫[*1)]

Radiation-induced Chondrosarcoma Arising 26 Years after Radiation Therapy for Rhabdomyosarcoma. Case Report

Toru UDAKA[*1)], Michiro SUSA[*1)], Robert NAKAYAMA[*1)], Itsuo WATANABE[*1)], Keisuke HORIUCHI[*1)], Ken HOSHINO[*2)], Tatsuo KURODA[*2)], Aya SASAKI[*3)], Makio MUKAI[*3)], Yoshiaki TOYAMA[*1)], Hideo MORIOKA[*1)]

臨整外 49：723～728，2014

Key words：軟骨肉腫(chondrosarcoma)，二次性悪性腫瘍(secondary malignant neoplasm)，放射線誘発性軟骨肉腫(radiation-induced chondrosarcoma)

患者は26歳の女性である．横紋筋肉腫に対する放射線照射後26年経過して骨盤軟骨肉腫を発症した．片側骨盤切除術を施行し，hip transposition法で再建した．術後1年の現在，局所再発は認めず，装具着用で片松葉杖歩行が可能である．横紋筋肉腫の放射線照射後に軟骨肉腫を生じた報告は，渉猟し得た範囲では2例と極めて稀であった．放射線治療後は肉腫の発生も考慮し長期の経過観察が必要と考えられた．

A 26-year-old woman developed a pelvic chondrosarcoma 26 years after radiation therapy for a rhabdomyosarcoma and was treated surgically by hemipelvectomy and reconstruction by a hip transposition procedure. There is no evidence of recurrence as of one year after surgery, and the patient is able to walk with a hip orthosis, and a crutch. Only two cases of radiation-induced chondrosarcoma after radiation therapy for a rhabdomyosarcoma have been reported in the English-language literature. We recommend that patients be followed up long term after radiation therapy in order to enable early detection of radiation-induced sarcomas.

はじめに

さまざまな悪性腫瘍に対する放射線治療後に，二次性に他の悪性腫瘍が発生することは広く知られている．放射線誘発性肉腫(radiation-induced sarcoma：RIS)は，放射線治療後長期の潜伏期を経て照射野内に二次的に悪性腫瘍が発生するもので，1922年にBeck[2)]によって報告されたのが最初である．Tountasら[9)]によると，放射線照射後，5年以上生存例で骨に発生した悪性腫瘍の頻度は0.04%程度とされている．RISの組織型については種々の報告があるが，骨肉腫や悪性線維

* 2013年12月17日受稿
*1) 慶應義塾大学医学部整形外科〔〒160-0016 東京都新宿区信濃町35〕Department of Orthopaedic Surgery, Keio University, School of Medicine
*2) 慶應義塾大学医学部小児外科　Department of Paediatric Surgery, Keio University School of Medicine
*3) 慶應義塾大学医学部病理診断部　Department of Pathology, Keio University, School of Medicine
本稿の概要は第46回日本整形外科学会骨・軟部腫瘍学術集会でポスター発表した．
＊利益相反：なし

©IGAKU-SHOIN Ltd, 2014

閲覧情報: 慶應義塾大学　信濃町メディアセンター 50322　2015/03/16 23:59:53

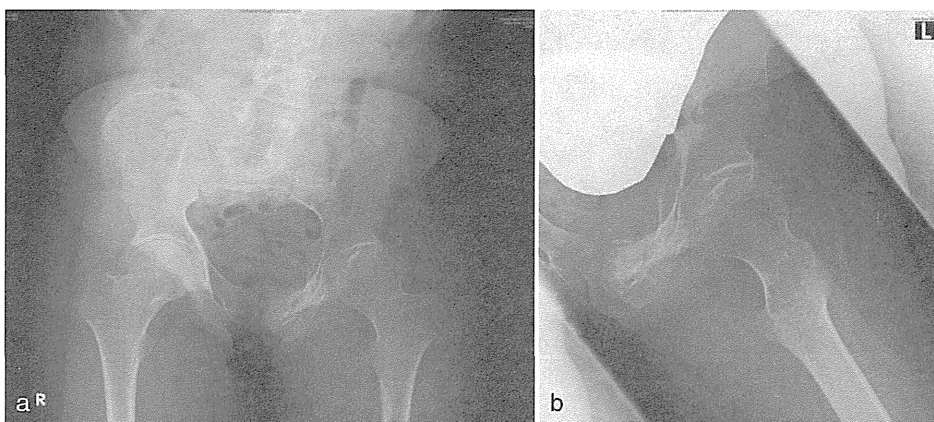

図1　単純X線像
a：正面　　b：ラウエンシュタイン法

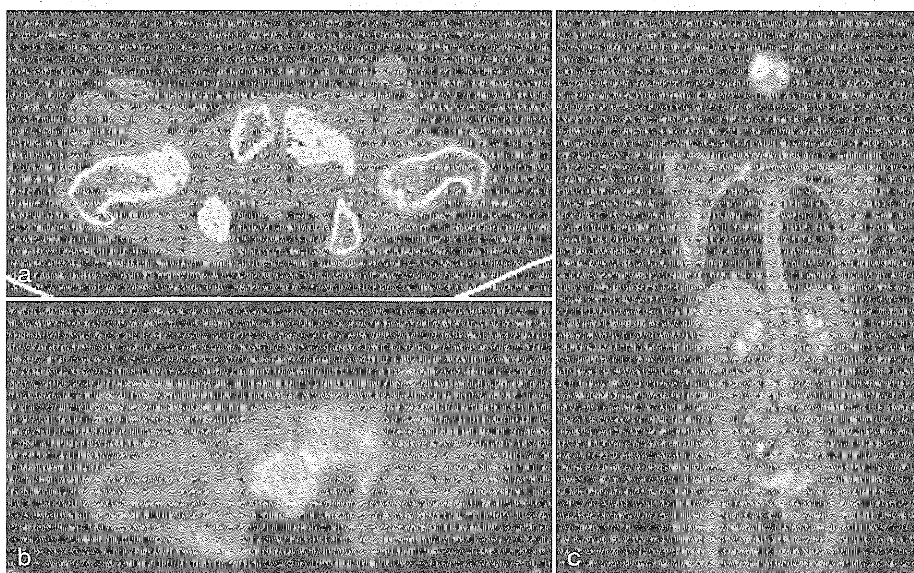

図2　CT像
a：単純CT　　b：PET-CT axial　　c：PET-CT coronal

性組織球腫(MFH)などの頻度が高いと言われている[8]. RISは，早期に，原発巣の再発や骨転移と鑑別し，適切な治療をすることが必要である．今回われわれは，横紋筋肉腫に対する治療後に発生した骨盤軟骨肉腫を経験したので，若干の文献的考察を加えて報告する．

症例

症例：26歳，女性

主訴：左股関節痛

現病歴：0歳3カ月で会陰部の横紋筋肉腫と診断され，手術と化学療法を施行後に放射線照射を合計30 Gy施行した．完全寛解と判断され，その後の経過観察においても再発は認められず経過良

閲覧情報: 慶應義塾大学　信濃町メディアセンター 50322　　2015/03/16 23:59:53

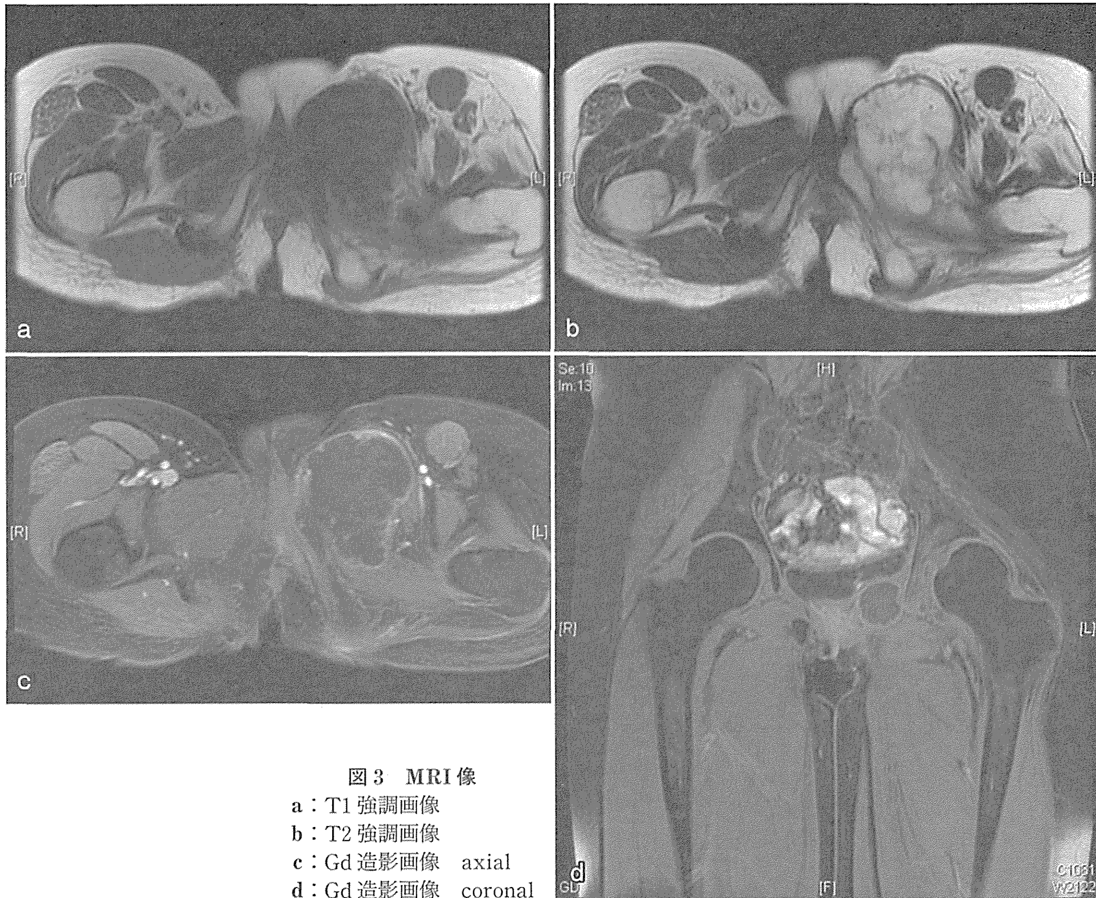

図3　MRI像
a：T1強調画像
b：T2強調画像
c：Gd造影画像　axial
d：Gd造影画像　coronal

好であった．26歳時に，左股関節の疼痛を自覚し，近医を受診した．X線，MRIで異常所見を認め，当科を紹介され受診した．

既往歴：0歳3カ月で髄膜瘤の手術，2歳で内反足の手術を施行した．

家族歴：特記すべき異常は認めなかった．

所見：左鼡径部に6 cm×4 cm大の弾性硬の腫瘤を触知し，腫脹，熱感，圧痛を認めた．股関節可動域には制限を認めなかった．

単純X線像：左恥骨に骨硬化像を認めた．また左臼蓋部に骨透亮像と硬化像の混在を認め，左大腿骨頭は軽度外方へ変位していた(図1-a，b)．

CT像：恥骨から臼蓋にかけて骨硬化，恥骨から連続する骨外腫瘤を認めた．骨外腫瘤の内部には部分的に石灰化も認めた(図2-a)．PET-CTでは左恥骨部の病変のSUVmaxが3.99で，他に明らかな遠隔転移は認めなかった(図2-b，c)．

MRI像：分葉状に発育するT1強調画像で低信号，T2強調画像で高信号，辺縁から淡く造影される8.8 cm×6.5 cm×5.5 cm大の腫瘍を認めた(図3)．

病理組織所見：切開生検術を施行したところ，軟骨基質の中に大小不同の異型核を有する細胞の増生を認め，軟骨肉腫Grade 2と診断した(図4)．

治療：片側骨盤切除術を施行し，hip transposition法で再建した(図5)．腫瘍は画像上，関節内への浸潤が疑われたため，関節包外切除を施行した．大転子は再度腫瘍用人工骨頭とスクリューで固定し，周囲軟部組織と逢着した．骨頭の安定性は，バイクリルメッシュ(ジョンソン・エンド・ジョンソン)を用いて腸骨骨切り部と逢縮することにより確保した．手術時間10時間38分，出血

閲覧情報: 慶應義塾大学　信濃町メディアセンター 50322　2015/03/16 23:59:53

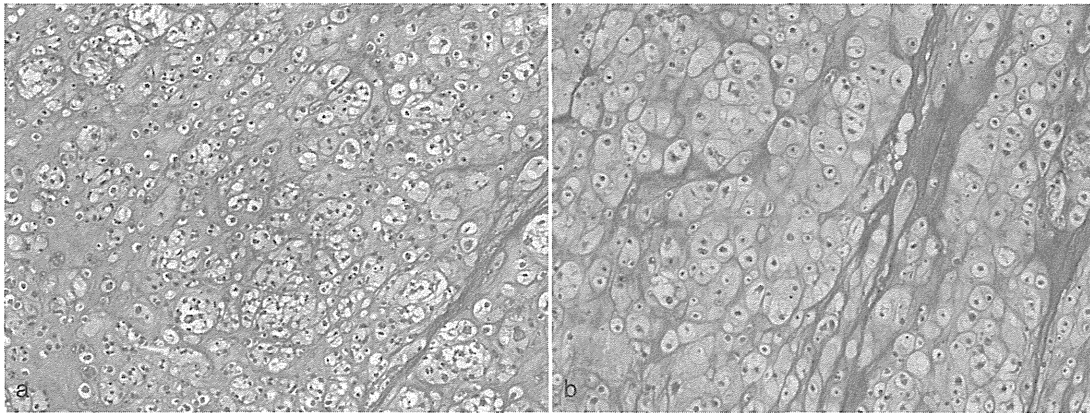

図4　病理組織(HE 染色)
a：弱拡大　b：強拡大

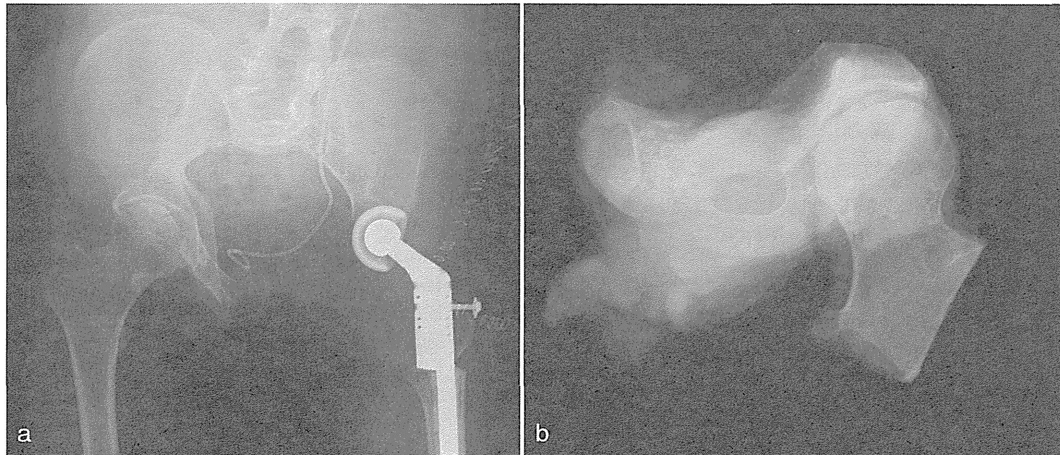

図5　術後画像所見
a：術後 X 線像　b：切除検体 X 線像

量は 680 g であった．術後 1 年の現在，局所再発は認めておらず，装具着用で，片松葉杖歩行が可能である．

考察

放射線誘発性肉腫は治療後，約 0.1%の割合で生じることが報告されている[1]．Cahan ら[3]のクライテリアでは，1)病理学的に，または放射線検査で骨内に前腫瘍病変を認めていないこと，2)放射線照射領域に肉腫の発生を認めること，3)放射線照射と肉腫の発生に十分に長い期間が存在すること，4)肉腫である病理学的証明，の 4 点が必要とされている[3]．本症例はこのクライテリアを満たしていた．

Wiklund ら[11]は 130 例の放射線誘発性肉腫を解析し，軟骨肉腫の発生頻度は 3.7%と報告しているが，横紋筋肉腫の放射線照射後に軟骨肉腫を生じた報告は，渉猟し得た範囲では 2 例と極めて稀であった[5,8](表 1)．また，放射線治療後の二次性悪性腫瘍の発生期間は 5〜50 年と，幅広く報告されている[10]．本症例は放射線治療後に軟骨肉腫を生じるまでの期間が 26 年と，既報告の 2 例と比べて 2 倍以上の年数が経過して発症していた．今後，がん患者の予後がさらに改善し，長期生存者が増加していくことが予想され，放射線治療後

閲覧情報: 慶應義塾大学　信濃町メディアセンター 50322　2015/03/16 23:59:53

表1　横紋筋肉腫の放射線照射後に軟骨肉腫を発症した症例

	年齢	初発癌の部位	化学療法	放射線治療	肉腫の発生部位	治療後の年数	経過
Peimer CA, et al	16	膀胱	アクチノマイシンD	24.5 Gy	右恥骨隆起	11年	9カ月後転移・再発なし
Heyn R, et al	16	縦隔	VAC	50.4 Gy	NA	12年10カ月	1年2カ月後死亡
本症例	26	会陰部	pulse VAC	30 Gy	左恥骨	26年	1年後転移・再発なし

VAC：アクチノマイシンD，ビンクリスチン，シクロフォスファミドの3剤併用療法

肉腫の発生も考慮し，長期の経過観察が肝要と考える．

放射線誘発性肉腫と特発性に発生した肉腫の予後の違いに関する報告は，これまで散見されるのみである．放射線誘発性軟骨肉腫に関しては，80人を解析したLagrangeら[7]の報告によれば，5年生存率は29%，平均生存期間は23カ月と短く，特発性の骨肉腫の5年生存率が約70%とされていることに比較すれば予後は悪いと考える．しかしながら放射線誘発性軟骨肉腫の報告例は極めて少ないため，特発性に発生した軟骨肉腫と比較した報告は認めていない．

骨盤腫瘍の切除後の再建についてはさまざまな方法が報告されている．関節固定術，人工関節置換術，flail hip，自家骨移植，切除した骨を処理骨として再利用するオートクレーブ法，パスツール法，放射線照射法，凍結法などが用いられているが，いずれの方法においても55～77%の高い合併症発症率が報告されている[4,6]．

骨盤部の病変では骨および周囲の筋肉を含む軟部組織の切除によって大きな死腔を生じるので，人工材料や処理骨・同種骨を使用する場合には術後感染率が高い．また，人工関節による再建では脱臼，弛みなどの危険性を伴い，長期的な耐用性には生物学的再建に劣る．処理骨，同種骨による再建では移植骨の吸収，骨折の危険性もある．広範切除後の骨盤再建法としてhip transposition法を用いることにより術後合併症の低減，良好な可動域の確保が可能と報告されている[6]．短所としては患肢の短縮などが挙げられる[4]．本症例においても術後1年の現在，局所再発は認めておらず，装具着用で片松葉杖歩行が可能である．

結語

今回，われわれは横紋筋肉腫に対する治療後，26年で生じた放射線誘発性軟骨肉腫の症例を経験した．放射線治療後は肉腫の発生も考慮し，長期の経過観察が肝要と考えられた．

文献

1) Amendola BE, Amendola MA, McClatchey KD, et al : Radiation-associated sarcoma : a review of 23 patients with postradiation sarcoma over a 50-year period. Am J Clin Oncol **12** : 411-415, 1989
2) Beck A : Zur Frage des Rontgensarkoms, zugleich ein Beitrag zur Pathogenese des Sarkoms. Munch Med Wochenschr **69** : 623-625, 1922
3) Cahan WG, Woodard HQ, Higinbotham NL, et al : Sarcoma arising in irradiated bone : report of eleven cases. 1948. Cancer **82** : 8-34, 1998
4) Gebert C, Gosheger G, Winkelmann W : Hip transposition as a universal surgical procedure for periacetabular tumors of the pelvis. J Surg Oncol **99** : 169-172, 2009
5) Heyn R, Haeberlen V, Newton WA, et al : Second malignant neoplasms in children treated for rhabdomyosarcoma. Intergroup Rhabdomyosarcoma Study Committee. J Clin Oncol **11** : 262-270, 1993
6) Hillmann A, Hoffmann C, Gosheger G, et al : Tumors of the pelvis : complications after reconstruction. Arch Orthop Trauma Surg **123** : 340-344, 2003
7) Lagrange JL, Ramaioli A, Chateau MC, et al : Sarcoma after radiation therapy : retrospective multiinstitutional study of 80 histologically confirmed cases. Radiation Therapist and Pathologist Groups of the Fédération Nationale des Centres de Lutte Contre le Cancer. Radiology **216** : 197-205, 2000

閲覧情報: 慶應義塾大学　信濃町メディアセンター 50322　2015/03/16 23:59:53

8) Peimer CA, Yuan HA, Sagerman RH : Post-radiation chondrosarcoma. A case report. J Bone Joint Surg Am **58** : 1033-1036, 1976
9) Tountas AA, Fornasier VL, Harwood AR, et al : Postirradiation sarcoma of bone : a perspective. Cancer **43** : 182-187, 1979
10) Walton A, Broadbent AL : Radiation-induced second malignancies. J Palliat Med **11** : 1345-1352, 2008
11) Wiklund TA, Blomqvist CP, Räty J, et al : Postirradiation sarcoma. Analysis of a nationwide cancer registry material. Cancer **68** : 524-531, 1991

閲覧情報: 慶應義塾大学 信濃町メディアセンター 50322 2015/03/16 23:59:53

Oncogene (2014) **33**, 5601–5608
© 2014 Macmillan Publishers Limited All rights reserved 0950-9232/14
www.nature.com/onc

ORIGINAL ARTICLE

PAX3-NCOA2 fusion gene has a dual role in promoting the proliferation and inhibiting the myogenic differentiation of rhabdomyosarcoma cells

H Yoshida[1,4], M Miyachi[1,4], K Sakamoto[1], K Ouchi[1], S Yagyu[1], K Kikuchi[1], Y Kuwahara[1], K Tsuchiya[1], T Imamura[1], T Iehara[1], N Kakazu[2], H Hojo[3] and H Hosoi[1]

We analyzed a complex chromosomal translocation in a case of embryonal rhabdomyosarcoma (RMS) and showed that it generates the fusion gene *PAX3* (paired box 3)-*NCOA2* (nuclear receptor coactivator 2). To understand the role of this translocation in RMS tumorigenesis, we established two types of stable mouse myoblast C2C12 cell lines expressing PAX3-NCOA2 and PAX3-FOXO1A (forkhead box O1A), respectively. Compared with control cells, PAX3-NCOA2 cells grew faster, were more motile, were less anchorage dependent, progressed more quickly through the G1/S phase of cell cycle and showed greater transcriptional activation of the PAX3 consensus-binding site. However, PAX3-NCOA2 cells proliferated more slowly and differentiated more weakly than did PAX3-FOXO1A cells. Both PAX3-NCOA2 cells and PAX3-FOXO1A cells formed tumors in nude mice, although the PAX3-NCOA2-induced tumors grew more slowly. Our results may explain why *NCOA2* rearrangement is mainly found in embryonal rhabdomyosarcoma, which has a better prognosis than alveolar rhabdomyosarcoma, which expresses the *PAX3-FOXO1A* fusion gene. These results indicate that the *PAX3-NCOA2* fusion gene has a dual role in the tumorigenesis of RMS: promotion of the proliferation and inhibition of the myogenic differentiation of RMS cells.

Oncogene (2014) **33**, 5601–5608; doi:10.1038/onc.2013.491; published online 11 November 2013

Keywords: rhabdomyosarcoma; PAX3-NCOA2; PAX3-FOXO1A; tumorigenesis; inhibiting differentiation

INTRODUCTION

Rhabdomyosarcoma (RMS) is the most common childhood soft tissue tumor. RMS can be divided into two main histopathological subgroups: embryonal rhabdomyosarcoma (ERMS) and alveolar rhabdomyosarcoma (ARMS). These subgroups differ considerably in their clinical phenotype and molecular features. The prognosis of ERMS is more favorable than that of ARMS. The majority of cases of the more aggressive ARMS are associated with one of two reciprocal translocations: t(2;13)(q35;q14), which generates an intronic fusion of *PAX3* (paired box 3) and *FOXOA1* (forkhead box O1A) that is also known as *FKHR* (forkhead in human rhabdomyosarcoma) and t(1;13)(p36;q14), which generates an intronic fusion of *PAX7* and *FOXOA1*.[1] The PAX3-FOXO1A translocation is associated with increased treatment failure and mortality rate.[2] PAX family members are transcription factors that regulate pattern formation during embryogenesis.[3] Several PAX genes, including *PAX3* and *PAX7*, contribute to tumorigenesis.[4] Pax3 is expressed in the developing nervous system and in somite compartments that give rise to skeletal muscle progenitors.[5,6] Exons 2, 3 and 4 of PAX3 encode the paired box, which is a distinctive feature of the PAX family, whereas the homeodomain is encoded by exons 5 and 6, and functions as a DNA-binding domain. Forkhead box (or *FOX*) genes have diverse roles including control of embryonic development and adult tissue-specific gene expression. FOXO1A has one transactivation domain (TAD) at the C-terminus,[7] and translocations between PAX3 and FOXO1A lead to an increase in transcriptional activation of the DNA-binding domains on PAX3. PAX3-FOXO1A induces cellular proliferation[8] and malignant transformation[9] and suppresses apoptosis.[10]

Recurrent *NCOA2* (nuclear receptor coactivator 2) gene rearrangements occur in ERMS.[11,12] Mosquera *et al.*[11] reported *NCOA2* gene rearrangements (*SRF-NCOA2* and *TEAD1-NCOA2*) in three cases of spindle cell RMS. Sumegi *et al.*[12] identified the fusion gene *PAX3-NCOA2* in each case of ERMS and ARMS that they investigated. We previously found a translocation involving chromosome band 2q35, which is the locus of the *PAX3* gene.[13] We later identified *NCOA2* as a candidate *PAX3* partner gene using fluorescence *in situ* hybridization (FISH). NCOA2 belongs to the p160 protein family, which also includes SRC-1 (steroid receptor coactivator), NCOA2/TIF2/ GRIP1/SRC-2 and pCIP/ACTR/AIB-1/RAC-3/TRAM-1/ SRC-3. NCOA2 has several functional domains including a PAS (sequence similarity with the Per Arndt-Sim motifs)/bHLH (sequence similarity with basic helix–loop–helix motifs) domain, a receptor interaction region, and two TADs.[14–17] NCOA2 is necessary for myogenic differentiation.[17] In nuclear receptor signaling, NCOA2 binds to nuclear receptors predominantly through its nuclear receptor-interacting domain (NID)[18,19] and recruits two transcriptional co-activators, CBP (CREB-binding protein)/p300 and CARM-1. CBP/p300 is recruited through its CBP interaction domain (CID/TAD1)[16,20] and CARM-1, an arginine

[1]Department of Pediatrics, Graduate School of Medical Science, Kyoto Prefectural University of Medicine, Kyoto, Japan; [2]Department of Environmental and Preventive Medicine, Shimane University School of Medicine, Shimane, Japan and [3]First Department of Pathology, Fukushima Medical University School of Medicine, Fukushima, Japan. Correspondence: H Hosoi, Department of Pediatrics, Graduate School of Medical Science, Kyoto Prefectural University of Medicine, Kajii-cho Hirokoji, Kamigyo-ku, Kyoto 602-8566, Japan.
E-mail: hhosoi@koto.kpu-m.ac.jp
[4]These authors contributed equally to this work.
Received 10 September 2013; accepted 20 September 2013; published online 11 November 2013

methyltransferase, is recruited through TAD2.[21–24] Sumegi et al.[12] demonstrated that deletion of TAD1 from PAX3-NCOA2 more strongly suppressed the transforming activity of the chimeric protein than did deletion of TAD2, and PAX3-NCOA2 needed an intact activation domain 2(TAD2) and CID for optimal transforming activity using the NIH3T3 mouse fibroblast cell line. Both TADs on NCOA2 boost transcriptional activation of PAX3-NCOA2, as they do in PAX3-FOXO1A.

However, the role of the *NCOA2* rearrangement including *PAX3-NCOA2* in RMS tumorigenesis remains to be elucidated. In this study, we compared the biological function of the *PAX3-NCOA2* fusion protein with *PAX3-FOXO1A* fusion protein to reveal the function of PAX3-NCOA2 in RMS tumorigenesis both *in vitro* and *in vivo*. To this end, we expressed these two fusion genes in C2C12 mouse myoblast cell lines and studied their biological character.

RESULTS

PAX3-NCOA2 was identified in an ERMS tumor specimen and transcriptional activation of the PAX3 consensus-binding site was enhanced

We previously showed the *PAX3* rearrangement in our case with ERMS by FISH analysis.[13] To identify the partner gene of *PAX3* in this case with the complex translocation involving 2q35 and 8q13, and so on, we narrowed down the 8q13 breakpoint region by stepwise FISH approach using bacterial artificial chromosome (BAC) probes located on chromosome 8q13. The results demonstrated that the BAC clone RP11-479K21 (located at 8q13.3) spanned the 8q13 breakpoint, and that the split signal of RP11-479K21 probe was fused to the signal of RP11-624P23 (on the telomeric side of the *PAX3* gene located at 2q35) (data not shown). RP11-479K21 clone contained the *NCOA2* gene. These results suggested that the candidate partner gene of *PAX3* was *NCOA2* in our case with ERMS. Sequence analysis of the *PAX3-NCOA2* PCR products of our patient's sample revealed that exon 7 of *PAX3* (391st AA) was fused to exon 12 (798th AA) of the *NCOA2* gene in-frame (Figure 1a). The resulting *PAX3-NCOA2* fusion protein consisted of the 391 N-terminal AA of PAX3 and the 666 C-terminal AA of NCOA2. A schema of the structures of intact and chimeric proteins is shown in Figure 1b. The *PAX3-NCOA2* fusion gene retained the DNA-binding domain of PAX3, and the CID/TAD1 and TAD2 domains of NCOA2, in agreement with the findings of Sumegi et al.[12] When HEK293 cells were transfected with the GFP-PAX3-NCOA2 expression vector, PAX3-NCOA2 localized in the nucleus (Figures 2a and b). The expressions of PAX3-NCOA2 enhanced transcriptional activation of the PAX3 consensus-binding site 3.8 times more than did the expression of the wild-type PAX3 and the expression of PAX3-FOXO1A enhanced it 19.8 times more (both $P<0.05$) (Figure 2c).

PAX3-NCOA2 stimulated proliferation and motility in myoblasts *in vitro*

We confirmed the protein expressions of PAX3-NCOA2 and PAX3-FOXO1A in HEK293 cells transiently transfected with FLAG-tagged constructs by western blotting (Figure 3a). Cell proliferation was assessed using C2C12 cells expressing PAX3-NCOA2, PAX3-FOXO1A or MSCV empty vector. On day 4, the numbers of PAX3-NCOA2 C2C12 cells and PAX3-FOXO1A C2C12 cells were 1.3 times more ($P<0.05$) and 1.7 times more ($P<0.05$), respectively, than the number of control cells (Figure 3b). The PAX3-NCOA2 cells switched from the G1phase to the S phase and showed an accelerated cell cycle progression (Figure 3c). Wound closure was more rapid with both the PAX3-NCOA2 cells and PAX3-FOXO1A cells than with the control cells (Figure 3d), indicating that the transformed cells have an enhanced motility. However, the wound width (% of original width) indicated that the PAX3-NCOA2 cells were not as motile as the PAX3-FOXO1A cells. When the cells were plated on soft agar, 3 ± 0.5 colonies grew from the control cells, whereas 53.6 ± 4.2 and 115.2 ± 0.5 colonies grew from the PAX3-NCOA2 cells and PAX3-FOXO1A cells (Figure 3f), respectively, indicating that both lines were capable of anchorage-independent growth. However, anchorage-independent growth of the PAX3-NCOA2 cells was only about half that of the PAX3-FOXO1A cells (Figure 3g).

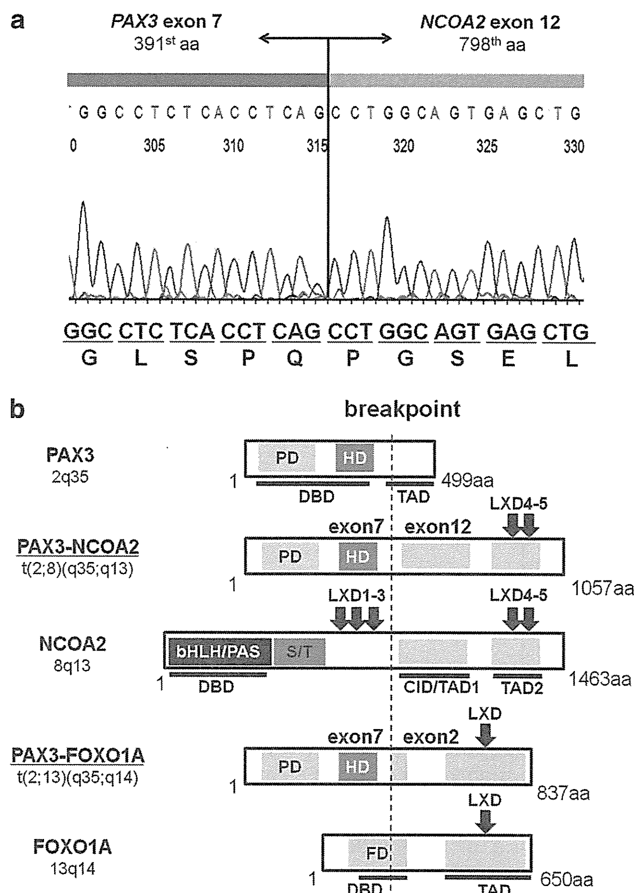

Figure 1. In-frame fusion of exon 7 of *PAX3* to exon 12 of *NCOA2*. (**a**) Representative RT–PCR and sequence analyses for chimeric transcripts in our patient. Sequence alignment of the *PAX3-NCOA2* breakpoint regions. Arrows depict the fusion point. Single-letter amino-acid code is displayed beneath the nucleotide sequence. (**b**) Comparison of wild type, fusion products associated with the t(2;8)(q35; q13) and t(2;13)(q35; q14) translocation. Interacting proteins are displayed as bars. The letters within the bars designate conserved domains (PD, paired domain; HD, homeodomain of the PAX3 protein; CID, CBP interaction domain; and bHLH/PAS, DNA-binding/protein heterodimerization domain, receptor nuclear translocator domain, involved in DNA binding). S/T represents the serine-threonine-rich region. Transcriptional domains of PAX3 are DBD (DNA-binding domain) and TAD (transcriptional activation domain). Arrows show the locations of LXXLL motifs in wild-type NCOA2, FOXO1A and their fusion proteins. NCOA2 has all five motifs, but the three on the N-terminus were lost during formation of PAX3-NCOA2. On the other hand, FOXO1A has only one motif, which is retained in PAX3-FOXO1A. All of the motifs on PAX3-NCOA2 (LXD4-5) and PAX3-FOXO1A (LXD) are in their transactivation domains. LXD, LXXLL-containing helical motif.

PAX3-NCOA2 inhibited the differentiation from myoblasts into myotubes in the differentiation medium

PAX3-NCOA2 and PAX3-FOXO1A morphologically blocked myotube differentiation (Figure 4a). Few of either PAX3-NCOA2

© 2014 Macmillan Publishers Limited

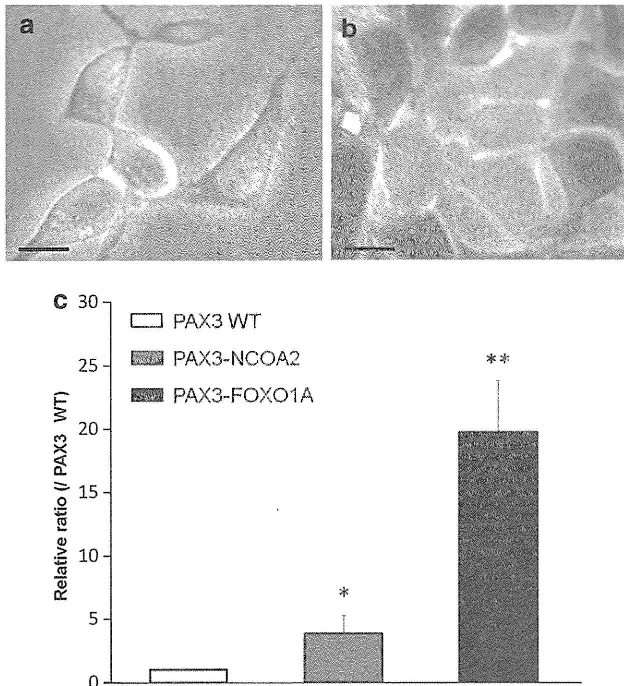

Figure 2. Confocal microscopy images showing localization of PAX3-NCOA2 in HEK293 cells. Cells were transfected with (**a**) GFP-PAX3-NCOA2 expression vector or (**b**) GFP empty vector. Scale bar, 20 μm. (**c**) Expression of PAX3-NCOA2 promoted transcriptional activation of PAX3 consensus-binding site by luciferase assay. Results represent the means ± s.d. of three independent experiments. **P*<0.05 and ***P*<0.01 compared with wild-type PAX3.

or PAX3-FOXO1A cells were stained with myosin heavy chain (MHC), a marker of muscle differentiation (Figure 4b). MHC positivity of PAX3-NCOA2-expressing cells and PAX3-FOXO1A-expressing cells were 2.3 ± 0.3% and 0.3 ± 0.3%, respectively, whereas the control cells was 53.0 ± 3.8% ($P<0.05$) (Figure 4c).

PAX3-NCOA2 promoted tumorigenesis *in vivo*

When fibroblasts expressing the fusion genes were transplanted into nude mice, the PAX3-NCOA2 and PAX3-FOXO1A cells took ~6.8 and 5.2 weeks, respectively, to form 15-mm-diameter tumors (Figure 5a). Therefore, tumorigenic properties of the PAX3-NCOA2 and PAX3-FOXO1A cell lines well reflect their *in vitro* anchorage-independent growth.

Every tumor was solid, firm and fibrotic. Unexpectedly, the tumors induced by the PAX3-NCOA2 and PAX3-FOXO1A cells did not differ with respect to any of eight characteristics examined: cell shapes, growth pattern/architecture, cellular cohesiveness, muscle differentiation, number of giant cells, nuclear-to-cytoplasm volume ratio reversal, hyperchromatism, cellular/nuclear pleomophism and stromal matrix. None of the tumors displayed the alveolar architectures on H&E stain and silver impregnation (Figure 5b, i–iii). All tumors were generally densely cellular and were mainly composed of a mixture of primitive RMS cells and limited numbers of nucleated giant cells and spindle-shaped tumor cells without myxoid stroma. All tumors stained positive for desmin, myoD1 and myogenin (Figure 5b, iv–vi), which are commonly used markers for RMS. Although some tumors showed evidence of local invasion, none of the tumor-bearing mice developed metastasis.

The LXXLL motifs of PAX3-NCOA2 was not required for anchorage-independent growth

The LXXLL motif (where L is leucine and X is any amino acid) is found in various co-activators, including NCOA[25,26] and FOXO family proteins, as well as in PAX3-NCOA2 and PAX3-FOXO1A (Figure 1b). To examine whether the LXXLL motif is involved in anchorage-independent growth, we constructed mutation/deletion constructs of the motif (Supplementary Table 1) following previous reports.[27,28] However, these mutations and deletions did not significantly affect anchorage-independent growth of either cell line (Figure 6), suggesting that the LXXLL motif is not a promising therapeutic target.

DISCUSSION

Our *in vitro* results revealed that the expression of PAX3-NCOA2 promoted transcriptional activation of the PAX3 consensus-binding site and that PAX3-NCOA2 actually acted as a transcriptional activator. PAX3-NCOA2 also enhanced proliferation, cell cycle progression, motility and anchorage-independent growth. In addition, we showed that PAX3-NCOA2 blocked myotube differentiation. These data indicated that PAX3-NCOA2 has a dual role in the tumorigenesis of RMS: promotion of cell proliferation and inhibition of myogenic differentiation. Our PAX3-NCOA2 results bear a close resemblance to previous findings that PAX3-FOXO1A promoted cell proliferation and motility and inhibited differentiation.[29–31] Our results suggest that PAX3-NCOA2 and PAX3-FOXO1A share the same mechanism for tumorigenesis. Finckenstein *et al.*[32] called *PAX3-FOXO1A* genes 'pangenes' in tumorigenesis, meaning that they simultaneously initiate myogenesis and inhibit terminal differentiation. It is not surprising that *PAX3-NCOA2* acts as a pangene like *PAX3-FOXO1A* because *PAX3-NCOA2* induces tumors derived from muscle tissue *in vivo*.

The tumors in nude mice derived from C2C12 cells transformed with PAX3-NCOA2 share several pathologic features with human ERMS tumor samples: the shapes of cells were small and round or spindle-like, and the cells having abundant cytoplasm were irregularly distributed among immature undifferentiated cells (Figure 5b, i–vi). Although PAX3-FOXO1A-expressing C2C12 cells developed non-invasive ERMS-like tumors in our experiment, Zhang *et al.*[33] showed that mouse myoblasts transformed with PAX3-FOXO1A-induced malignant, ARMS-like tumors in mice. In addition, almost all PAX3-FOXO1A tumor-bearing mice develop spontaneous metastasis to the lungs, one of the targeted sites for metastasis in human ARMS. On the other hand, Wang *et al.*[34] reported that a PAX3-FOXO1A stable cell line formed tumors but the tumors did not have alveolar structure and did not invade any organ, in agreement with our results. As suggested by Naini *et al.*[35], whether or not a tumor is malignant with alveolar structure may depend on not only PAX3-FOXO1A but also one or more other abnormalities as well, loss of p16INK4A/p14ARF or overexpression of MYCN.

Sumegi *et al.*[12] did not report the prognosis of his patients with the *PAX3-NCOA2* fusion gene. However, our case had localized RMS, responded to standard therapy and is alive and in remission at 9 years after treatment. Mosquera *et al.*[11] also reported recurrent *NCOA2* rearrangements in spindle cell-type RMS, which is a subtype with good prognosis. In all of our experiments, the most aggressive phenotype was PAX3-FOXO1A, followed by PAX3-NCOA2, as expected. The finding that the PAX3-NCOA2 stable cell line expressed a less aggressive phenotype than did the PAX3-FOXO1A stable cell line supports our hypothesis that RMS with the *PAX3-NCOA2* fusion gene has a better prognosis than RMS with the *PAX3-FOXO1A* fusion gene.

The LXXLL motif was originally observed in cofactor proteins that interact with hormone-activated nuclear receptors.[25]

© 2014 Macmillan Publishers Limited

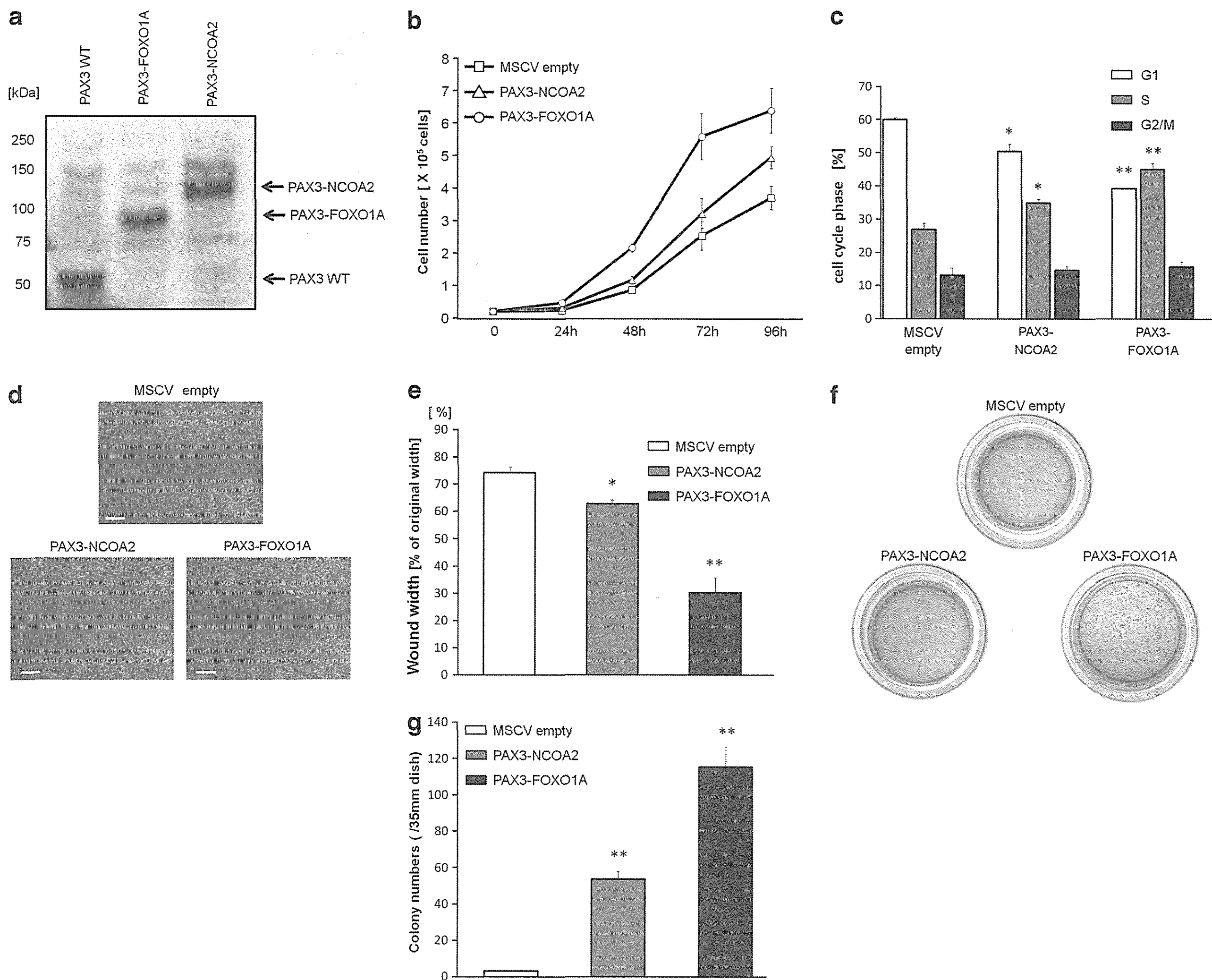

Figure 3. Promotion of some characteristics of tumorigenesis by PAX3-NCOA2. (**a**) Western blot showing expressions of intact and chimeric genes. The molecular weights of wild-type PAX3, PAX3-FOXO1A, and PAX3-NCOA2 were 53, 97 and 120 kDa, respectively. (**b**) Cell growth of C2C12 with and without the chimeric gene 96 h later. Results represent the means ± s.d. from three independent experiments. (**c**) Cell cycle of C2C12 with and without the chimeric gene 72 h later as determined by flow cytometry. Results represent the means ± s.d. of three independent experiments. **P* < 0.05 and ***P* < 0.01 compared with the same phase of MSCV empty vector. (**d**) Light microscopic images of C2C12 cells that were scratched using a pipette tip and compared the wound width 6 h later. Scale bar, 100 μm. (**e**) Average wound widths, expressed as a percent of the original width, obtained from 30 measurements in each photo. PAX3-NCOA2 enhances motility of mouse myoblasts. Results represent the means ± s.d. of three independent experiments. **P* < 0.05 and ***P* < 0.01 compared with MSCV empty vector. (**f**) Photographs of colonies of C2C12 cells with and without the chimeric gene 14 days later. (**g**) Anchorage-independent growth of the three cell types using a colony-forming soft agar assay as described in Materials and methods. Results represent the means ± s.d. of three independent experiments. ***P* < 0.01 compared with MSCV empty vector.

Functionally active examples of LXXLL motifs have also been documented in proteins that do not directly interact with nuclear receptors, including several transcription factors,[36,37] cAMP (cyclic adenosine monophosphate) response element-binding protein (CREB)-binding protein (CBP) and p300,[38] and mediator subunits. In fact, PAX3-NCOA2 has two LXXLL motifs. Deguchi *et al.*[28] constructed LXXLL mutants and deletions of *MOZ-TIF2* fusion protein, and demonstrated that these abnormalities contributed to decrease anchorage-independent growth and transcriptional activity in murine bone marrow cells. On the other hand, PAX3-FOXO1A has only one LXXLL motif. Mutating it was found to decrease the transcriptional activity of FOXO1A in simian virus-40-transformed hepatocytes.[27] However the LXXLL motif did not have a key role in our experimental system using a mouse myoblast cell line transduced with human chimeric genes. This difference might be due to a difference of cell types or to a difference in the conformation of the chimeric proteins.

In conclusion, our study has two main findings: the *PAX3-NCOA2* fusion gene 1) has a dual role in the tumorigenesis of RMS, promoting cell proliferation and inhibiting myogenic differentiation and 2) is less aggressive than the *PAX3-FOXO1A* fusion gene. PAX3-NCOA2 could be a potential marker of low risk in RMS. The analyses needed to determine the risk stratification and prognostic factors of RMS have progressed from classic morphology to molecular diagnoses, using aberrant chimeric genes. The present results should help provide a more rational stratification of RMS.

MATERIALS AND METHODS

Tumor tissue samples

Tumor specimens from our patient with ERMS were surgically resected before any chemotherapy and immediately stored at −80 °C. The patient's symptoms are described elsewhere.[13] Written informed consent was given by the parents according to the protocol approved by the institutional

© 2014 Macmillan Publishers Limited

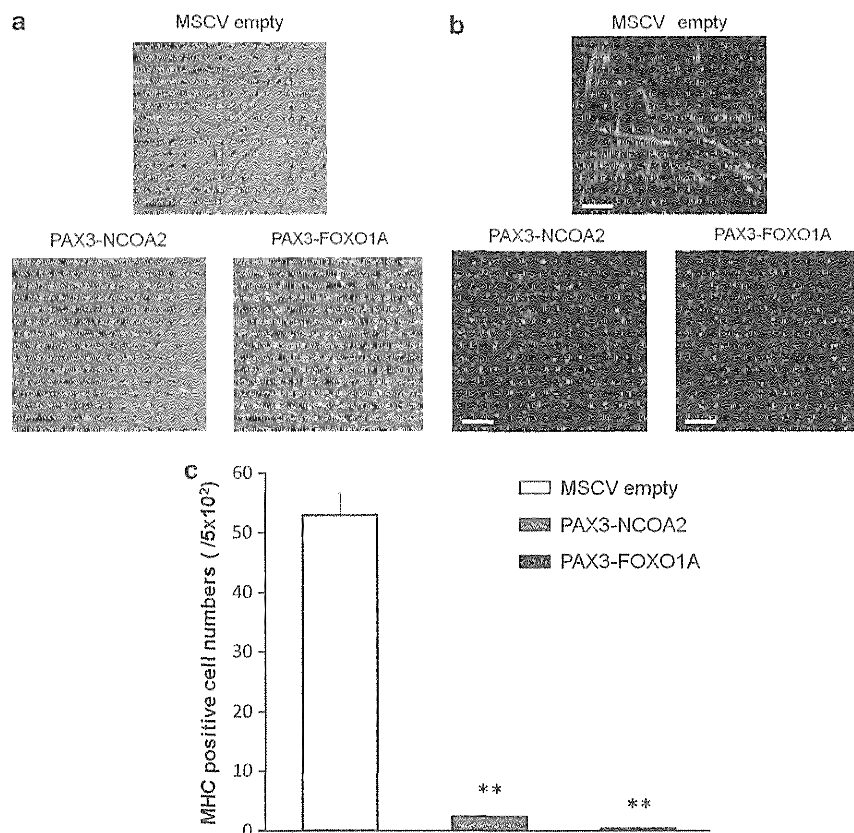

Figure 4. Inhibition of myogenic differentiation by PAX3-NCOA2 and PAX3-FOXO1A. (**a**) Representative light microscopic images of mouse myoblasts with MSCV vector alone (control), cells expressing PAX3-NCOA2 and cells expressing PAX3-FOXO1A after 4 days in differentiation medium (DM). Scale bar, 50 μm. The MSCV empty cells formed multinuclear fusion myotubes, while the PAX3-NCOA2 and PAX3-FOXO1A formed only a few fusion cells. (**b**) Fluorescent images of MHC staining after 4 days in DM. Scale bar, 100 μm. Representative images of MSCV empty showed MHC and DAPI (for nuclei), meanwhile that of PAX3-NCOA2 and PAX3-FOXO1A demonstrated few MHC-positive cells. (**c**) Numbers of MHC-positive cells per 5.0×10^2 cells. Results represent the means ± s.d. of three independent experiments. $^{**}P < 0.01$ compared with MSCV empty vector.

review board of Kyoto Prefectural University of Medicine in accordance with the Declaration of Helsinki.

FISH analysis

The BAC clones (RP11 series) were selected according to the University of California Santa Cruz Genome Browser (http://genome.ucsc.edu) and were obtained from Invitrogen (Basel, Switzerland). These BAC DNAs were isolated using a NucleoBond BAC 100 kit (Macherey-Nagel Inc., Easton, PA, USA) and were directly labeled by means of nick translation with SpectrumGreen-dUTP or SpectrumOrange-dUTP (Abbott Molecular/Vysis, Des Plaines, IL, USA). Hybridization, washing and detection were performed using standard procedures. FISH images were captured and analyzed with the PowerGene system (Applied Imaging, Santa Clara, CA, USA).

Cell cultures, transfection, infection and reagents

Mouse myoblast C2C12 cells and human embryonic kidney HEK293 were purchased from the American Type Culture Collection (Manassas, VA, USA). These cells were maintained in growth medium: Dulbecco's modified Eagle's high-glucose medium, supplemented with 10% fetal bovine serum, penicillin (100 U/ml) and streptomycin (10 mg/ml) at 37 °C in a humidified atmosphere of 5% CO_2. Stable C2C12 cell lines expressing PAX3-NCOA2, and PAX3-FOXO1A were established using a murine stem cell virus (MSCV) retrovirus expression system (Clontech Laboratories Inc., Madison, WI, USA). C2C12 cells were transfected in 60-mm dishes at ~50% confluence with 1 μg of purified expression vector DNA, 8 μl of Enhancer and 7.5 μl of Effectene (Qiagen, Hombrechtikon, Switzerland) in 1 ml of Dulbecco's modified Eagle's high-glucose medium. After 48 h, the cells were trypsinized and replanted at a 1: 5 dilution in medium. Selection of stability transfected cells was performed with 1000 μg/ml of G418 sulfate (Life Technologies, Carlsbad, CA, USA).

Reverse transcription–polymerase chain reaction (RT–PCR) and direct sequencing of PAX3-NCOA2

Total RNA was extracted from a tumor specimen with the use of an RNeasy mini kit (Qiagen) according to the manufacturer's instructions. Complementary DNA (cDNA) was synthesized with the use of the SuperScript First-Strand Synthesis System for RT–PCR (Invitrogen) according to the manufacturer's instructions. The fusion region of *PAX3-NCOA2* was PCR amplified in overlapping fragments. The primer pairs used in this experiment are listed in Supplementary Table 2. The entire coding region of PAX3-NCOA2 was PCR amplified. PCR products were sequenced with the use of the BigDye Terminator v3.1 Cycle Sequencing kit (Applied Biosystems, Rotkreuz, Switzerland) and the ABI PRISM 377 Sequence Detection System (Applied Biosystems).

Localization assay

HEK293 cells were transfected with GFP (green fluorescent protein)-PAX3-NCOA2 expression vector and the fusion protein was observed with confocal microscopy BZ-8000 (KEYENCE, Osaka, Japan).

Assay for cell proliferation

C2C12 cell lines expressing each gene or MSCV vector alone were seeded at 2×10^4 cells/well. Every 24 h, an aliquot of the cells was lysed under hypotonic conditions, and nuclei were counted with a Coulter counter (ERMA Inc., Jacksonville, FL, USA) until 96 h later (day 4).

Cell cycle analysis

Cells were plated for 72 h and then washed twice with 1 × PBS and then incubated for 30 min with propidium iodide (PI) to stain DNA. Propidium

© 2014 Macmillan Publishers Limited

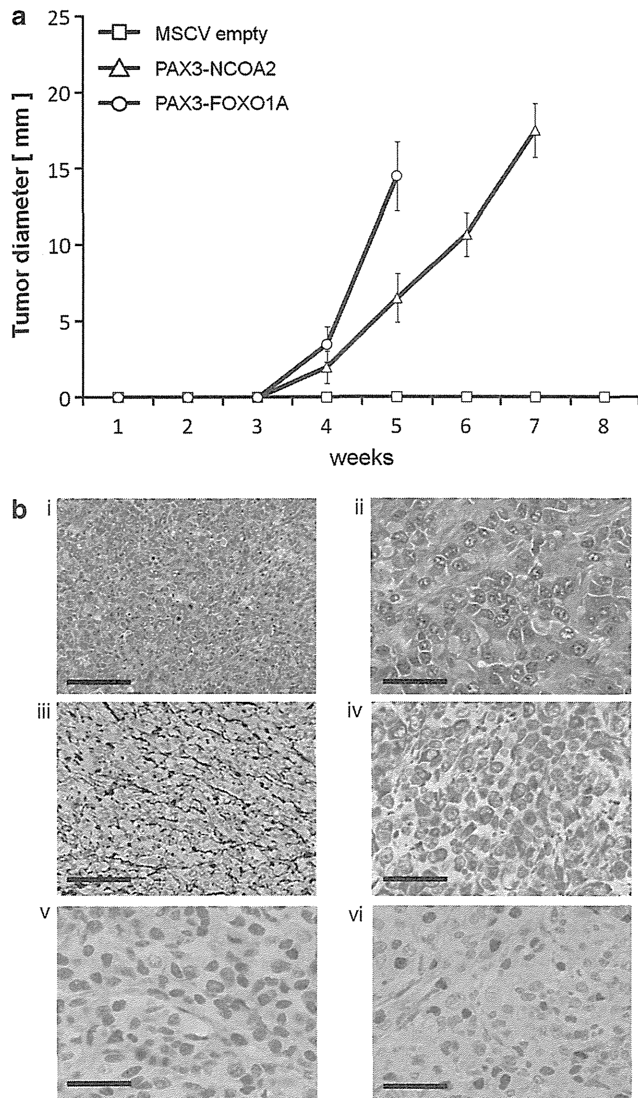

Figure 5. Effects of PAX3-NCOA2 and PAX3-FOXO1A on the proliferation of C2C12 cells in a murine xenograft model. (**a**) C2C12 cell were injected into subcutaneous tissue of BALB/c nude mice. Tumor diameters were measured every 2 or 3 days. Each point represents the means ± s.d. of three independent experiments. (**b**) Images representative of tissue sections of PAX3-NCOA2 stained with H&E (i, ii), silver impregnation (iii) and with antibodies specific for desmin (iv), myoD1 (v) and myogenin (vi). Scale bar, 200 μm (i, iii) and 100 μm (ii, iv–vi), respectively. The tumor cells ranged from small round cells to large elongated poorly differentiated cells, and exhibited varying degrees of myogenic differentiation. There were small oval or long spindle-shaped differentiated rhabdomyoblasts with eosinophilic cytoplasm, without cross striation. Even in silver impregnation (iii), there was no alveolar architecture. Also lacking was the classic cystic pattern with tumor cells palisaded against fibrovascular stroma. None of the cells were anaplastic. In the immunohistology, desmin, myoD1 and myogenin were positive; however, the expressions of myoD1 and myogenin were different. Thus, the latter differentiation in rhabdomyogenesis appeared to be abnormal or suppressed.

iodide fluorescence was read on a FACS Calibur (BD Biosciences, Franklin Lakes, NJ, USA), and the data were analyzed with Cell Quest software (BD Biosciences). The cell cycle phase was determined on the basis of DNA content using the ModFit LT Software (Verity Software House, Topsham, ME, USA) as described previously.[39]

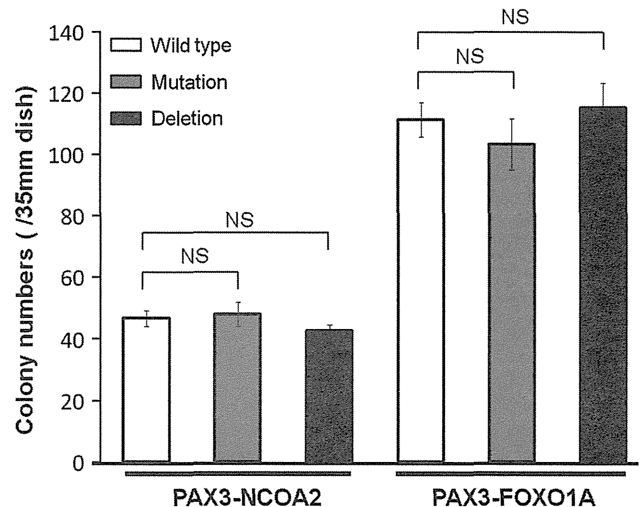

Figure 6. Effect of mutations and deletions of the LXXLL motif on anchorage-independent growth of PAX3-NCOA2 and PAX3-FOXO1A cells using a colony-forming soft agar assay. Results represent the means ± s.d. of three independent experiments. A *P*-value of less than 0.05 was considered statistically significant; NS, no significance.

Anchorage-independent soft agar colony formation assay

Cells were cultured in a two-layer soft agar system developed by Hambruger *et al.*[40] It consisted of a 1% Noble agar underlayer and a 0.7% Noble agar overlayer containing 2×10^4 cells in 35-mm dishes. Colonies were allowed to form for duration of 2 weeks with fresh media added every 3 days. Plates were stained with crystal violet and colonies more than 0.1 mm in diameter were counted.

Luciferase reporter assay for PAX3-FOXO1A enhancer

A luciferase reporter construct was generated by inserting multimerized PAX3 DNA-binding sites (6 × e5 DNA-binding sites) into pGL3 vector. A total of 1×10^5 HEK293 cells were plated per 35-mm plate and cotransfected 24 h later with FLAG expression vectors, pGL3 basic 6 × e5 vector and pRL-TK vector; 290, 90 and 20 μg, respectively. Luciferase activity was determined by using a dual luciferase assay system (Promega, Wallisellen, Switzerland) to adjust for differences in transfection efficiency. Data shows luciferase expression relative to pFLAG wild-type PAX3.

Western blot

Cells were lysed with Laemmli sample buffer. Protein concentrations in the cell lysates were measured with the Bio-Rad DC Protein Assay (Bio-Rad Laboratories, Hercules, CA, USA). Samples were boiled for 5 min in sample buffer containing bromophenol blue and 1 × β-ME, and equal amounts of protein were separated by sodium dodecylsulfate–polyaclylamide gel electrophoresis (SDS–PAGE). Electrophoretic separation was carried out on 10% polyacrylamide gel (Bio-Rad Laboratories), and the proteins were subsequently transferred to an Immobilon-P membrane (Millipore, Billerica, MA, USA). Membranes were blocked in PBST (phosphate-buffered saline with Tween 20) with 5% non-fat dry milk powder and incubated with the following primary antibodies: FLAG (Sigma-Aldrich, St Louis, MO, USA). The membranes were then washed with PBST and incubated with goat anti-mouse secondary antibody (GE Healthcare, Little Chalfont, UK) or anti-rabbit (GE Healthcare). Antibody binding was detected with the enhanced chemiluminescence detection system (ECL and ECL plus; GE Healthcare).

Assays for the differentiation of myoblast and immunofluorescence

To initiate myogenesis, cells were rinsed thoroughly with phosphate-buffered saline (PBS) before adding differentiation medium; Dulbecco's modified Eagle's high-glucose medium containing 2% Horse serum, penicillin (100 U/ml), and streptomycin (10 mg/ml) 24 h after seeding (day 1). Differentiated cells were observed on day 4 with a confocal microscope BZ-8000 (KEYENCE) to assess morphological change. For immunofluorescence, cells on cover slips were fixed with absolute

© 2014 Macmillan Publishers Limited

methanol, washed and incubated with anti-myosin heavy chain antibody (Sigma-Aldrich) for 1 h, rinsed with PBS, incubated with fluorescein isothiocyanate-conjugated anti-mouse IgG (Invitrogen) for 1 h, and visualized using a fluorescence microscope as previously described.[41]

Wound-healing assay

The cell layers were scratched using a pipette tip, and then cultured in the differentiation medium. Immediately after scratching (0 h), the plates were photographed and the distance between the edges of the wound area was measured and defined as 100%. At 6 h after scratching, the plates were photographed and the distance between the edges of the wound region was again measured and presented as a percentage of the distance between the edges of wound area at 0 h.

In vivo tumorigenesis

Tumors were induced in 4- to 6-week-old male athymic nude mice (BALB/c nu/nu; SHIMIZU Laboratory Supplies, Kyoto, Japan). Each mouse was injected subcutaneously with 2×10^6 C2C12 cells suspended in 0.5 ml of PBS at a single site to the lower flank. Tumor diameter was monitored every 2 or 3 days on onset of tumor formation. Mice were killed when the tumor size reached 17 mm in diameter. At the end point of the experiments, tumors were extracted and immediately photographed. A portion of the tumor was embedded in paraffin for histopathological and immunohistochemical analyses. At least three mice were used in each experiment. The mice used for this study were handled in strict adherence with local governmental and institutional animal care regulation.

Histopathology and immunohistochemistry

Histological specimens were fixed in 10% formalin and routinely processed for embedding in paraffin. Histological sections 4-μm-thick were stained with hematoxylin and eosin (H&E), silver impregnation or hybridized to antibodies specific for desmine, myoD1 and myogenin. Slides were reviewed by a board-certified pathologist (H Hojo) to define the histologic type of cancer. The sections were incubated with anti-desmin, anti-myoD1 and anti-myogenin antibody that was diluted at 1:20, 1:25 and 1:50 respectively. Sections were then treated with a VECTASTAIN Elite ABC kit (Vector Laboratories, Burlingame, CA, USA).

Mutant and deletion construction

The LXXLL motif of NCOA2 was mutagenized by inverse PCR using Topo-PAX3-NCOA2-vector with *Xho*I and *Bam* HI tags as a template. The PCRs were initiated with a 2-min incubation at 95 °C followed by 10 cycles of 95 °C for 30 s, 60 °C for 30 s and 72 °C for 7 min, and finally 10 min incubation at 72 °C. The template plasmid was digested with *Dpn* I for 1 h at 37 °C, and the remaining PCR products were treated with restriction enzymes *Xho*I and *Bam* HI. A total of 7.5 μl MSCV vector and insert DNA with 7.5 μl Ligation high ver.2 were ligated with a DNA Ligation Kit Ligation high Ver.2 (Toyobo, Osaka, Japan) according to the manufacturer's instructions. Thereafter, the composed plasmid was transformed into competent cells, and MSCV vector containing these cDNAs was generated by transfecting C2C12 cells. Mutagenesis/deletion of the LXXLL motifs of PAX3-NCOA2 and PAX3-FOXO1A were performed in the same way. The primer pairs used in this study are listed in Supplementary Table 2.

Statistical analysis

Statistical analysis was performed using the unpaired Student's *t*-test. A *P*-value of less than 0.05 was considered statistically significant.

ABBREVIATIONS

ARMS, alveolar rhabdomyosarcoma; BAC, bacterial artificial chromosome; bHLH, sequence similarity with basic helix–loop–helix motifs; CBP, CREB-binding protein; cDNA, complementary DNA; CID, CBP interaction domain; CREB, cAMP (cyclic adenosine monophosphate) response element-binding protein; DM, differentiation medium; ERMS, embryonal rhabdomyosarcoma; FISH, fluorescence *in situ* hybridization; FKHR, forkhead in human rhabdomyosarcoma; FOXO1A, forkhead box O1A; G1, Gap1; GFP, green fluorescent protein; H&E, hematoxylin and eosin; LXD, LXXLL-containing helical motif; MHC, myosin heavy chain; MSCV, murine stem cell virus; NCOA2, nuclear receptor coactivator 2; NID, nuclear receptor-interacting domain; PAS, sequence similarity with the Per Arndt-Sim (PAS) motifs; PAX3, paired box 3; PBS, phosphate-buffered saline; PBST, phosphate-buffered saline with Tween 20; PI, propidium iodide; RMS, rhabdomyosarcoma; RT–PCR, reverse transcription–polymerase chain reaction; SDS–PAGE, sodium dodecylsulfate–polyacrylamidegel electrophoresis; TAD, transactivation domain

CONFLICT OF INTEREST

The authors declare no conflict of interest.

ACKNOWLEDGEMENTS

This work was supported by Grant-in-aid for Scientific Research (A) 21249085, (A) 25253095, (B) 22390239, (C) 22591166, Grant-in-aid for Young Scientists (B) 24791078 and Grant-in-aid for Project for Development of Innovative Research on Cancer Therapeutics from the Ministry of Education, Culture, Sports, Science and Technology of Japan.

REFERENCES

1 Galili N, Davis RJ, Fredericks WJ, Mukhopadhyay S, Rauscher 3rd FJ, Emanuel BS *et al.* Fusion of a fork head domain gene to PAX3 in the solid tumour alveolar rhabdomyosarcoma. *Nat Genet* 1993; **5**: 230–235.
2 Sorensen PH, Lynch JC, Qualman SJ, Tirabosco R, Lim JF, Maurer HM *et al.* PAX3-FKHR and PAX7- FKHR gene fusions are prognostic indicators in alveolar rhabdomyosarcoma: a report from the Children's Oncology Group. *J Clin Oncol* 2002; **20**: 2672–2679.
3 Tremblay P, Gruss P. Pax: genes for mice and men. *Pharmacol Ther* 1994; **61**: 205–226.
4 Robson EJ, He SJ, Eccles MR. A PANorama of PAX genes in cancer and development. *Nat Rev Cancer* 2006; **6**: 52–62.
5 Goulding MD, Chalepakis G, Deutsch U, Erselius JR, Gruss P. Pax-3, a novel murine DNA binding protein expressed during early neurogenesis. *EMBO J* 1991; **10**: 1135–1147.
6 Jostes B, Walther C, Gruss P. The murine paired box gene, Pax7, is expressed specifically during the development of the nervous and muscular system. *Mech Dev* 1990; **33**: 27–37.
7 Barr FG. Gene fusions involving PAX and FOX family members in alveolar rhabdomyosarcoma. *Oncogene* 2001; **20**: 5736–5746.
8 Anderson J, Ramsay A, Gould S, Pritchard-Jones K. PAX3-FKHR induces morphological change and enhances cellular proliferation and invasion in rhabdomyosarcoma. *Am J Pathol* 2001; **159**: 1089–1096.
9 Lam PY, Sublett JE, Hollenbach AD, Roussel MF. The oncogenic potential of the Pax3-FKHR fusion protein requires the Pax3 homeodomain recognition helix but not the Pax3 paired-box DNA-binding domain. *Mol Cell Biol* 1999; **19**: 594–601.
10 Bernasconi M, Remppis A, Fredericks WJ, Rauscher 3rd FJ, Schafer BW. Induction of apoptosis in rhabdomyosarcoma cells through down-regulation of PAX proteins. *Proc Natl Acad Sci USA* 1996; **93**: 13164–13169.
11 Mosquera JM, Sboner A, Zhang L, Kitabayashi N, Chen CL, Sung YS *et al.* Recurrent NCOA2 gene rearrangements in congenital/infantile spindle cell rhabdomyosarcoma. *Genes Chromosomes Cancer* 2013; **52**: 538–550.
12 Sumegi J, Streblow R, Frayer RW, Dal Cin P, Rosenberg A, Meloni-Ehrig A *et al.* Recurrent t(2;2) and t(2;8) translocations in rhabdomyosarcoma without the canonical PAX-FOXO1 fuse PAX3 to members of the nuclear receptor transcriptional coactivator family. *Genes Chromosomes Cancer* 2010; **49**: 224–236.
13 Hosoi H, Kakazu N, Konishi E, Tsuchihashi Y, Hada S, Amaya E *et al.* A novel PAX3 rearrangement in embryonal rhabdomyosarcoma. *Cancer Genet Cytogenet* 2009; **189**: 98–104.
14 Hong H, Kohli K, Trivedi A, Johnson DL, Stallcup MR. GRIP-1 a novel mouse protein that serves as transcriptional coactivator in yeast for the hormone binding domains of steroid receprtors. *Proc Natl Acad Sci USA* 1996; **93**: 4946–4952.
15 Voegel JJ, Heine MJ, Zechel C, Chambon P, Gronemeyer H. TIF2, a 160 kDa transcriptional mediator for the ligand dependent activation function AF-2 of nuclear receptors. *EMBO J* 1996; **15**: 3667–3675.
16 Voegel JJ, Heine MJ, Tini M, Vivat V, Chambon P, Gronemeyer H. The coactivator TIF2 contains three nuclear receptor-binding motifs and mediates transactivation through CBP bindingdependent and -independent pathways. *EMBO J* 1998; **17**: 507–519.
17 Chen SL, Dowhan DH, Hosking BM, Muscat GE. The steroid receptor coactivator, GRIP-1, is necessary for MEF-2C-dependent gene expression and skeletal muscle differentiation. *Genes Dev* 2000; **14**: 1209–1228.

© 2014 Macmillan Publishers Limited

18 Ding XF, Anderson CM, Ma H, Hong H, Uht RM, Kushner PJ *et al.* Nuclear receptor-binding sites of coactivators glucocorticoid receptor interacting protein 1 (GRIP1) and steroid receptor coactivator 1 (SRC-1): multiple motifs with different binding specificities. *Mol Endocrinol* 1998; **12**: 302–313.
19 Berrevoets CA, Doesburg P, Steketee K, Trapman J, Brinkmann AO. Functional interactions of the AF-2 activation domain core region of the human androgen receptor with the amino-terminal domain and with the transcriptional coactivator TIF2 (transcriptional intermediary factor2). *Mol Endocrinol* 1998; **12**: 1172–1183.
20 Ma H, Hong H, Huang SM, Irvine RA, Webb P, Kushner PJ *et al.* Multiple signal input and output domains of the 160-kilodalton nuclear receptor coactivator proteins. *Mol Cell Biol* 1999; **19**: 6164–6173.
21 Chen D, Ma H, Hong H, Koh SS, Huang SM, Schurter BT *et al.* Regulation of transcription by a protein methyltransferase. *Science* 1999; **284**: 2174–2177.
22 Chen D, Huang SM, Stallcup MR. Synergistic, p160 coactivatordependent enhancement of estrogen receptor function by CARM1 and p300. *J Biol Chem* 2000; **275**: 40810–40816.
23 Teyssier C, Chen D, Stallcup MR. Requirement for multiple domains of the protein arginine methyltransferase CARM1 in its transcriptional coactivator function. *J Biol Chem* 2002; **277**: 46066–46072.
24 Lee YH, Coonrod SA, Kraus WL, Jelinek MA, Stallcup MR. Regulation of coactivator complex assembly and function by protein arginine methylation and demethylimination. *Proc Natl Acad Sci USA* 2005; **102**: 3611–3616.
25 Heery DM, Kalkhoven E, Hoare S, Parker MG. A signature motif in transcriptional co-activators mediates binding to nuclear receptors. *Nature* 1997; **387**: 733–736.
26 McInerney EM, Rose DW, Flynn SE, Westin S, Mullen TM, Krones A *et al.* Determinants of coactivator LXXLL motif specificity in nuclear receptor transcriptional activation. *Genes Dev* 1998; **21**: 3357–3368.
27 Nakae J, Cao Y, Daitoku H, Fukamizu A, Ogawa W, Yano Y *et al.* The LXXLL motif of murine forkhead transcription factor FoxO1 mediates Sirt1-dependent transcriptional activity. *J Clin Invest* 2006; **116**: 2473–2483.
28 Deguchi K, Ayton PM, Carapeti M, Kutok JL, Snyder CS, Williams IR *et al.* MOZ-TIF2-induced acute myeloid leukemia requires the MOZ nucleosome binding motif and TIF2-mediated recruitment of CBP. *Cancer Cell* 2003; **3**: 259–271.
29 Calhabeu F, Hayashi S, Morgan JE, Relaix F, Zammit PS. Alveolar rhabdomyosarcoma-associated proteins PAX3/FOXO1A and PAX7/FOXO1A suppress the transcriptional activity of MyoD-target genes in muscle stem cells. *Oncogene* 2013; **32**: 651–662.
30 Jothi M, Nishijo K, Keller C, AKT Mal AK. and PAX3-FKHR cooperation enforces myogenic differentiation blockade in alveolar rhabdomyosarcoma cell. *Cell Cycle* 2012; **11**: 895–908.
31 Kikuchi K, Tsuchiya K, Otabe O, Gotoh T, Tamura S, Katsumi Y *et al.* Effects of PAX3-FKHR on malignant phenotypes in alveolar rhabdomyosarcoma. *Biochem Biophys Res Commun* 2008; **365**: 568–574.
32 Finckenstein FG, Shahbazian V, Davicioni E, Ren YX, Anderson MJ. PAX-FKHR function as pangenes by simultaneously inducing and inhibiting myogenesis. *Oncogene* 2008; **27**: 2004–2014.
33 Zhang Y, Schwartz J, Wang C. Comparative analysis of paired- and homeodomain-specific roles in PAX3-FKHR oncogenesis. *J Clin Exp Pathol* 2009; **2**: 370–383.
34 Wang W, Kumar P, Wang W, Epstein J, Helman L, Moore JV *et al.* Insulin-like growth factor II and PAX3-FKHR cooperate in the oncogenesis of rhabdomyosarcoma. *Cancer Res* 1998; **58**: 4426–4433.
35 Naini S, Etheridge KT, Adam SJ, Qualman SJ, Bentley RC, Counter CM *et al.* Defining the cooperative genetic changes that temporally drive alveolar rhabdomyosarcoma. *Cancer Res* 2008; **68**: 9583–9588.
36 Parker D, Rivera M, Zor T, Henion-Caude A, Radhakrishnan I, Kumar A *et al.* Role of secondary structure in discrimination between constitutive and inducible activators. *Mol Cell Biol* 1999; **19**: 5601–5607.
37 Litterst CM, Pfitzner E. An LxxLL motif in thetransactivation domain of STAT6 mediates recruitment of NCoA-1/SRC-1. *J Biol Chem* 2002; **277**: 36052–36060.
38 Torchia J, Rose DW, Inostroza J, Kamei Y, Westin S, Glass CK *et al.* The transcriptional co-activator p/CIP binds CBP and mediates nuclear-receptor function. *Nature* 1997; **387**: 677–684.
39 Livak KJ, Schmittgen TD. Analysis of relative gene expression data using real-time quantitative PCR and the 2(-DD C(T)) method. *Methods* 2001; **25**: 402–408.
40 Hamburger AW, Salmon SE, Kim MB, Trent JM, Soehnlen BJ, Alberts DS *et al.* Direct cloning of human ovarian carcinoma cells in agar. *Cancer Res* 1978; **38**: 4118–4130.
41 Tsuchiya K, Hosoi H, Misawa-Furihata A, Houghton PJ, Sugimoto T. Insulin-like growth factor-I has different effects on myogenin induction and cell cycle progression in human alveolar and embryonal rhabdomyosarcoma cells. *Int J Oncol* 2007; **31**: 41–47.

Supplementary Information accompanies this paper on the Oncogene website (http://www.nature.com/onc)

© 2014 Macmillan Publishers Limited

■ The Japanese Journal of Pediatric Hematology/Oncology vol. 51(5): 439–445, 2014

【第55回日本小児血液・がん学会学術集会】教育セッション1：軟部組織腫瘍

横紋筋肉腫治療研究の現況

細井　創[1,2*]

[1] 京都府立医科大学大学院医学研究科小児発達医学
[2] 日本横紋筋肉腫研究グループ（JRSG）代表

要　旨

横紋筋肉腫の層別化治療研究の現況と課題について概説する．1）低リスクA群：米国では，シクロホスファミド1.2 g/m² のVAC療法4サイクル後VA療法4サイクルのみの大胆な減量短縮治療が試験され，成績低下のない結果を得ようとしている．2）低リスクB群：シクロホスファミド2.2 g/m²/サイクルの強化VAC療法で著明な生存率の改善をみたが，患児に不妊や二次癌を引き起こす可能性が高く，治療中，死に至る重篤な肝障害venoocclusive disease（VOD）も発生した．その後シクロホスファミド1.2 g/m² のVAC療法4サイクル後VA療法12サイクルという大胆な減量治療が試験されたが，成績は低下する模様である．3）中間リスク群：トポテカンを用いたIRS-Vでは対照とした強化VAC療法と有意差はなく，その後行われたシクロホスファミド1.2 g/m² のVACとVI（ビンクリスチンとイリノテカン）の交替療法の結果が待たれる．4）高リスク群：全生存率は約30%で過去25年間改善がない．米国で行われた多剤併用強化療法は治療開始18か月FFS 66%と改善を認めたが36か月で32%にまで下がり，良好な寛解導入率を維持するプラスアルファの治療が模索されている．

キーワード：横紋筋肉腫，臨床研究
Key words: rhabdomyosarcoma, clinical studies

I　はじめに

横紋筋肉腫は小児で最も頻度の高い軟部組織肉腫である．その生存率は，近年の集学的治療の進歩により，飛躍的に改善した[1-5]．治療成績の向上は，1）迅速で正確な中央病理診断システムの導入，2）病期・術後分類のみならず，発生部位や病理組織亜型を加味した横紋筋肉腫独自のリスク分類の策定，3）初期治療の導入法や化学療法・外科手術・放射線治療のタイミング，化学療法各サイクルの治療開始・休止基準を詳細に規定した臨床試験計画書（プロトコル）に基づく多施設共同層別化治療研究の成果の積み重ねに依るところが大きい．層別化治療のためのリスク分類では，今後，強力な予後不良因子として，病理組織型とは独立して，特異的融合遺伝子の有無がさらに重要視されていくであろう[6-9]．生存率の改善とともに治療の長期の影響（晩期合併症）が顕在化し，とくに低・中間リスク群では，その軽減と防止が次の目標となっている[10-16]．低リスク群では治療の軽減と短縮化が，中間リスク群では新規薬剤導入により，蓄積毒性のある単一薬剤の繰り返し使用による晩期合併症の軽減を，また，未だ治療成績の改善の少ない高リスク群では分子標的治療薬や抗体療法，免疫療法らの追加投与によって長期的寛解維持，治癒が目指されている[8]．また，トランレーショナルリサーチとして，本腫瘍の病態解明およびそれに基づく分子標的治療薬の開発が試みられている[17-25]．本疾患の治療成績改善と治療後の患者QOLのさらなる向上のためには，予後をより反映したリスク群分類ときめ細かな層別化治療法の確立，また病態に基づく，より有効で安全な治療薬の開発が必要であるが，今後は，その希少性ゆえ，国際的共同治療研究が必要となるであろう．本稿では，米国とわが国の横紋筋肉腫治療研究の現況と今後の展望について概説する．

II　リスク分類

図1上に，世界的に最も歴史が古く，大規模な横紋筋肉腫治療研究グループである米国Intergroup Rhabdomyosarcoma Study Group（IRSG）の第5世代臨床研究（IRS-V：1997年～2004年）のリスク分類を示す．病理組織亜型，術前病期分類（Stage），術後グループ分類（Group）と年齢により，低リスクA，低リスクB，中間リスク，高リスクの4つのリスク群に分類され，層別化治療研究が行われた[5]．

IRSGはその後，米国Children Oncology Group（COG）に組み込まれ，Soft Tissue Sarcoma Study（STS）committeeとして，第6世代以降のスタディを続けている．図1下に最近のSTSのリスク分類を示す[8,9]．第5世代（IRS-V）スタディでは低リスクB群であった集団の一部が低リスクA群に相当するLow subset 1に含まれ，従来中間リスク群であった10歳未満の胎児型Group IVが高リスク群に分類されている[26]．

2014年7月24日受付，2014年7月24日受理
* 別刷請求先：〒602-8566 京都市上京区河原町通広小路上る梶井町465
京都府立医科大学小児科学教室　細井　創

IRS-V リスク分類

胎児型	I	II a NO NX	II b N1	II c N1	III 眼窩 NO NX	III 眼窩 N1	III 眼窩以外 NO NX	III 眼窩以外 N1	IV
1(予後良好部位)	Low A					Low B			
2(不良部位)									
3(不良部位)		Low B				Intermediate			
4(遠隔転移)									10歳未満 Inter / 10歳以上 High

胞巣型	I	II a NO NX	II b N1	II c N1	III 眼窩 NO NX	III 眼窩 N1	III 眼窩以外 NO NX	III 眼窩以外 N1	IV
1(予後良好部位)					Intermediate				
2(不良部位)									
3(不良部位)									
4(遠隔転移)									High

JRS-I リスク分類

胎児型	I	II a NO NX	II b N1	II c N1	III 眼窩 NO NX	III 眼窩 N1	III 眼窩以外 NO NX	III 眼窩以外 N1	IV
1(予後良好部位)	Low A					Low B			
2(不良部位)									
3(不良部位)		Low B				Intermediate			
4(遠隔転移)									High

胞巣型	I	II a NO NX	II b N1	II c N1	III 眼窩 NO NX	III 眼窩 N1	III 眼窩以外 NO NX	III 眼窩以外 N1	IV
1(予後良好部位)					Intermediate				
2(不良部位)	Int.								
3(不良部位)						High			
4(遠隔転移)									High

ARST 0331, 0431, 0531 (IRS-VI) リスク分類

胎児型	I	II a NO NX	II b N1	II c N1	III 眼窩 NO NX	III 眼窩 N1	III 眼窩以外 NO NX	III 眼窩以外 N1	IV
1(予後良好部位)	Low subset 1					Low subset 2			
2(不良部位)									
3(不良部位)	Low subset 2					Intermediate			
4(遠隔転移)									High

胞巣型	I	II a NO NX	II b N1	II c N1	III 眼窩 NO NX	III 眼窩 N1	III 眼窩以外 NO NX	III 眼窩以外 N1	IV
1(予後良好部位)									
2(不良部位)									
3(不良部位)					Intermediate				
4(遠隔転移)									High

図1　横紋筋肉腫のリスク分類の変遷．上にIRS-Vのリスク分類を，中央にJRS-Iのリスク分類を，下にIRS-VI（ARST）に相当するCOG-STSのリスク分類を示す．JRS-Iでは，IRS-Vでは中間リスク群とされた，胎児型Group IV/10歳未満の患者と胞巣型Stage 2, 3/Group IIIの患者は高リスク群に分類した．COG-STSリスク分類では，IRS-Vで高リスク群に分類された10歳未満のGroup IV胎児型横紋筋肉腫は高リスク群に含められ，試験された．

わが国では，2000年初頭，日本横紋筋肉腫研究グループ（Japan Rhabdomyosarocma Study group; JRSG）が結成された．筆者らが事前に行った後方視的調査結果[27]をもとに，上記を図1中のようにIRSGリスク分類を改変し，2004年より，横紋筋肉腫の全国スタディが開始された．

III　低リスクA群

低リスクA群は，胎児型横紋筋肉腫例のうち，予後良好部位に発生し（Stage 1），1）初回手術で組織学的完全摘除できた例（Group I），あるいは2）組織学的残存があるが領域リンパ節転移のない例（Group IIa），もしくは3）眼窩発生例で領域リンパ節転移のない肉眼的腫瘍残存例（Group III），あるいは4）予後不良部位発生例で腫瘍径が5 cm以下かつ領域リンパ節転移がなく（Stage 2），組織学的完全摘除ができた（Group I）例である（図1上，中）．COG-STSでは，従来低リスクB群の一部であったStage 1 Group IIB，CまたはStage 2/Group IIの胎児型横紋筋肉腫も，IRS-IVスタディでは低リスクA群に劣らぬ好成績であったことから，IRS-VIに相当するARST0331プロトコルからは，上記群も低リスクA群（Low subset 1）として分類して（図1下）試験治療を行っている[3,4,26]．

表1に示す通り，本群に対し，IRS-IVスタディでは，1サイクル投与量2.2 g/m^2×12サイクル（総投与量26.4 g/m^2）のシクロホスファミドを加えた強化VAC療法（治療期間約1年）を試験し，5年無再発生存率（FFS）93%と，IRS-IIIスタディで本群に行われたビンクリスチンとアクチノマイシンDによるVA療法の5年FFS 83%に比して有意な改善を認めた[3,4]．ただし，本試験中にVODによる死亡例が続発し，投与量，投与方法の変更を余儀なくされた[10,11]ことや，シクロホスファミドの総投与量が男性・女性ともに不妊必発の高投与量である[28]ことから，本治療が最終的標準治療とはみなされず，IRS-VIに相当する本群を対象とするCOG-STS臨床試験（ARST0331）プロトコルでは，シクロホスファミドは1サイクル1.2 g/m^2×4サイクル（総投与量4.8 g/m^2），あとはVAを4サイクル繰り返す総期間24週間のVAC/VA療法という大胆な減量ならびに治療期間の短縮が試みられた[29]．結果は，未だ2年の段階ではあるが，無再発生存率が88%とIRS-IVと遜色ない結果がでている[29]．本プロトコルは，妊孕能が担保できる比較的少量のCPM投与量であること，治療期間も約6か月と従来になく短いこと等を考慮すれば，低リスクA群の最終的標準治療となる可能性がある．

わが国では，JRSGの低リスクA群プロトコル（JRS-I低リスクA）として，シクロホスファミド1サイクル1.2 g/m^2×8サイクル（総投与量9.6 g/m^2）のVAC療法を試験し，3年無再発生存率において92%（3年全生存率100%）と好成

表1　低リスクA群の試験治療と成績の変遷

スタディ	VCR サイクル	ActD サイクル	CPM サイクル	VCR mg/m²	ActD mg/m²	CPM mg/m²	5年 FFS	p値	5年 OS	p値
IRS-III	36	6		72	13.5		83%	0.03	93%	0.12
IRS-IV	32	10	12	48	22.5	26.4	93%		98%	
IRS-V (D9602)	36	16		54	24		89%			
ARST331	18	8	4	27	12	4.8	88%（2年）		99%（2年）	

表2　低リスクB群の試験治療と成績の変遷

スタディ	VCR サイクル	ActD サイクル	CPM サイクル	VCR mg/m²	ActD mg/m²	CPM mg/m²	5年 FFS	p値	5年 OS	p値
IRS-III	36	6		72	13.5		70%	0.008	79%	0.004
IRS-IV	32	10	12	48	22.5	26.4	84%		95%	
IRS-V (D9602)	36	16	13	54	24	28.6	85%			
ARST0331 (IRS-VI)	36	16	4	54	21.6	4.8	66%（3年）		83%（3年）	

績を得ている（未発表データ）．今年度から実施予定の次期JRS-IIスタディでは，ARST0331と同様の低リスクA群分類と同様のVAC/VA療法にさらに治療軽減し，JRS-Iでの好成績を落とさず，さらなる治療減量が可能か検証予定である．

IV　低リスクB群

低リスクB群は，胎児型横紋筋肉腫例のうち，予後良好部位に発生し（Stage 1），1）領域リンパ節転移のある組織学的残存腫瘍例（Group IIbまたはIIc），または2）領域リンパ節転移の有無にかかわらず，肉眼的残存腫瘍のある（Group III）眼窩発生以外の例，あるいは3）予後不良部位に発生するも領域リンパ節転移のない，腫瘍径5 cm以下（Stage 2）の例で，組織学的残存ありの初回手術をうけた（Group IIa）例，あるいは4）予後不良部位に発生した腫瘍径が5 cm以上か，領域リンパ節転移のある（Stage 3）例で，組織学的完全摘除（Group I）もしくは組織学的残存手術（Group II）のできたものである（図1上，中）．ARST033以降はStage 1/Group IIB，CまたはStage 2/Group IIは低リスクA群に含め臨床試験を行っていることは上記に述べた通りである（図1下）．

表2に示す通り，IRS-IVスタディでは，1サイクル投与量2.2 g/m²×12サイクル（総投与量26.4 g/m²）のシクロホスファミドを加えた強化VAC療法（治療期間約1年）を試験し，5年無再発生存率（FFS）84%と，IRS-IIIスタディで本群に行われたビンクリスチンとアクチノマイシンDによるVA療法の5年FFS 70%に比べ，有意な改善を認めた[4]．ただし，重篤なVODの副作用[10,11]や，シクロホスファミドの総投与量が男性・女性ともに不妊必発の高投与量である[28]ことから，IRS-VIに相当するCOG-STS臨床試験（ARST0331）プロトコルでは，本群には1サイクル1.2 g/m²のシクロホスファミドを4サイクル（総投与量4.8 g/m²）行い，あとはVAを11サイクル行うだけの大胆な減量VAC/VA療法が試験された．結果は，3年無再発生存率66%とIRS-IVやIRS-V（D9602）に比し，明らかな成績低下を示した[30]．彼らはこの群を今後，中間リス群に含めて試験を行うことも考慮している．

わが国では，この群に2.2 g/m²/サイクルのシクロホスファミドを用いたVAC療法を8サイクルに8サイクルのVA療法を加えるVAC/VA療法（総シクロホスファミド投与量17.6 g/m²）を試験した．2012年に最終登録を終え，現在さらに3年の観察期間中である．今年度から実施予定のJRS-IIスタディでは，この群には1.2 g/m²のシクロホスファミドを用いたVAC療法とビンクリスチンと塩酸イリノテカン（VI）療法の交替療法（総シクロホスファミド投与量10.8 g/m²）を試験する予定である．

V　中間リスク群

中間リスク群は，胎児型横紋筋肉腫例のうち，予後不良部位に発生し（Stage 2，3），初回手術で肉眼的残腫瘍のある（Group III）例，あるいは胞巣型横紋筋肉腫例のうち，遠隔転移のないすべての例である（図1下）．高リスク群に実験的なウィンドウスタディを組み込んでいたIRS-Vでは，比較的予後良好の10歳未満の遠隔転移（Group IV）のある胎児型横紋筋肉腫例は，中間リスク群に含めていた[31]（図1上）が，IRS-VIに相当するARST0431プロトコルからは高リスク群でもウィンドウスタディはなくなった

ため，病理組織型や年齢を問わず，遠隔転移のある（Group IV）すべての例が高リスク群に分類されるようになった[8,9]（図1下）．

実際，強化VAC療法（シクロホスファミド2.2 g/m²/サイクル）を施行したIRS-Vスタディでは，Stage 2，3/Group III胎児型横紋筋肉腫の4年無再発生存率は76%，Stage 1，2/Group I，IIおよびStage 1，2/Group IIIの胞巣型横紋筋肉腫の5年無再発生存率は，それぞれ80%と76%（1歳以上であれば83%）と良好であり，これらの群は引き続き，中間リスク群として治療研究を行うことが妥当であろう[31]．一方，原発腫瘍が大きい（長径5 cm以上），あるいは領域リンパ節転移のある（Stage 3）/Group I，II胞巣型横紋筋肉腫の5年無再発生存率は66%であり，Stage 3/Group IIIのそれは45%（なかでも領域リンパ節転移のあるものは31%）とさらに不良であり[32,33]，胞巣型Stage 3/Group III例，なかでも領域リンパ節転移のあるものは高リスク群に含めるべきかもしれない．

IRS-VIに相当するCOG-STS中間リスク群プロトコル（ARST0531）では，シクロホスファミド1.2 g/m²/サイクルのVAC療法を対照として，同様のVACサイクルとビンクリスチンおよび塩酸イリノテカン（VI）サイクルの交替療法が比較検討された[8]．この背景には，IRS-IVやIRS-Vスタディで用いたシクロホスファミド2.2 g/m²/サイクルの強化VAC療法では，重篤なVODの急性毒性[10,11]や長期の影響として不妊が必発のシクロホスファミドの総投与量である[28]ことから，その軽減を試みたものであるが，中間解析では，無再発生存率はVAC療法の対照群とVAC/VI療法群で有意差なく，有効性としてVAC/VI療法のVAC療法との同等性が示唆されたが，絶対的な治療成績としては，IRS-Vの中間リスク群のそれよりやや低下する可能性が懸念されており，今後の結果と評価が待たれる．

COG-STSの次期中間リスク群臨床試験としては，Low subset 2（JRSGの低リスクB群に相当）を中間リスク群に加え，VAC/VI療法を対照として，これにmTOR阻害剤のtemosirolimusを追加した治療法を比較検討することが計画されている．この根拠としては，塩酸イリノテカンとmTOR阻害剤の組み合わせによる前臨床試験（動物実験）で相乗効果が示されている[34]こと，再発例のスタディで，ビノレルビンとシクロホスファミドにtemosirolimusを加えた群とVEGF阻害剤のbevacizumabを加えた群との比較試験で前者の優位性が示されたことによる．

わが国では，2004年から行われたJRS-Iスタディで，IRS-Vに順じ，2.2 g/m²/サイクルのシクロホスファミドによるVACを14サイクル（総投与量30.4 g/m²，VOD対応の投与方法修正あり）の強化VAC療法（治療期間約1年）を追試し，3年無進行生存率（PFS）70%以上，3年全生存率80%以上の良好な結果を得ている（主任研究者 太田茂先生のご厚意による情報提供）．ただし，先にも述べた通り，JRS-Iの中間リスク群には比較的予後不良のStage 2，3/Group III胞巣型横紋筋肉腫が含まれない（JRS-Iでは高リスク群とした）こと，生存例の妊孕能は期待できない多量のシクロホスファミド総投与量であることは留意すべきである．

わが国では，次期JRS-II中間リスク群では，シクロホスファミド2.2 g/m²/サイクルのVACとVIの交替療法でシクロホスファミド総投与量を18.8 g/m²まで減量しても治療成績が下がらないかを試験する予定である．本シクロホスファミド総投与量は，少なくとも年少女児においてはその妊孕能を保持できる可能性のある投与量設定である．

VI　高リスク群

高リスク群は，現在，COG-STSでは「初診時遠隔転移のある（Stage 4/Group IV）横紋筋肉腫」と定義されている（図1下）．ただし，前述した通り，COG-STSで中間リスク群に含められているStage 3/Group III胞巣型横紋筋肉腫は，その5年無再発生存率が45%である[32,33]ことから高リスク群に含めて試験研究を行うことを考慮すべきかもしれない．また，領域リンパ節転移がある（N1）胞巣型横紋筋肉腫の5年無再発生存率についても，領域リンパ節転移のないものの5年無再発生存率約75%に比べ，約40%と明らかに予後不良である（IRS-IVスタディにおける胞巣型204例の解析）ことから治療強化が必要と考えられ，今後，高リスク群として治療研究を行うべきかもしれない[32,33]．実際，ヨーロッパ中心のSIOPスタディでは胞巣型N1例は高リスク群に分類され，臨床試験が行われている．

10歳未満のStage 4/Group IV胎児型横紋筋肉腫はIRS-Vでは中間リスク群に分類されたが，最近のCOG試験のデータでは，10歳未満，10歳以上ともに3年無再発生存率50～60%であり，中間リスク群としてよりは高リスク群として治療研究をするのが妥当であろう．

Stage 4/Group IV胞巣型横紋筋肉腫の3年無再発生存率は極めて不良であり，高リスク群とすることに異論のないところであり，本群は従来とは全く新しい治療ストラテジーが必要な一群と言える．

2006年に開始されたCOG-STSの高リスク群プロトコルARST0431は，2週間隔のVDCとIE療法にVI療法やVAC療法を組み合わせた多剤併用化学療法が骨格で，2年足らずで予定症例数を達し，治療開始後18か月（治療終了後約6か月）の無再発生存率は66%（胎児型80%，胞巣型57%）とこれまでにない良好な早期成績により大きな期待がもたれたが，治療開始後36か月では32%（胎児型50～62%，胞巣型18%）まで低下するという残念な結果であった．そこで，彼らは，2010年から開始した次期スタディARST08P1では，ARST0431を基本骨格としてtemozolomide

やIGF-I受容体抗体，あるいはその両方をアドオンした治療を3者比較するパイロットスタディを行った[8]．その結果が待たれる．次次期スタディではpazopanibをアドオンした試験が検討されている．

わが国のJRS-Iスタディで，初診時遠隔転移のある（Stage 4/Group IV）横紋筋肉腫例以外にStage2，3/Group III例を加えて高リスク群とし，cisplatin，cyclophosphamaide，pirarubicin，etoposide，ifosfamide，actinomycin-Dを用いた多剤併用療法で寛解導入し，thiotepaとmelphlanで末梢血幹細胞移植を利用した超大量療法を行うレジメンを施設限定で試験した．結果は，胞巣型Stage 2，3/Group IIIの3年無進行生存率は50%あまり，Stage 4/Group IVのそれは40%あまりであり，従来のIRSスタディやCOGスタディより良好な結果となる可能性がある（主任研究者 原純一先生のご厚意による情報提供）．ただし，超大量療法で用いたthiotepaが現在製造中止であるため本治療法は現在は実施ができない．

わが国では，JRS-I高リスク群臨床試験が登録終了後，各施設判断で行われたARST0431に準じたレジメンで寛解導入後WT1免疫ワクチン療法を追加した患者に長期生存例があることが経験されており，ARST0431レジメンをベースに寛解維持療法として，HLA適応例にはWT1免疫ワクチン療法，HLA不適応例にはCOG-STS再発プロトコルで有効性を示されたビノレルビンとシクロホスファミド療法を追加する臨床試験を作成中である．

VII　血清遊離筋特異的マイクロRNA，*miR-206*の横紋筋肉腫の診断，治療反応性評価および予後予測マーカーとしての有用性

現在まで横紋筋肉腫特異的な血清腫瘍マーカーは存在しなかった．近年，タンパク質に翻訳されない非コードRNA（microRNA：以下miRNA）の存在が明らかになり，その発現プロファイルは組織や腫瘍特異的であることが報告されている[35,36]．小児がんにおいても細胞株を用いた検討で，発現プロファイルが腫瘍により異なるとする報告がある[37]．また，小児で最も頻度の高い軟部肉腫である横紋筋肉腫の細胞株では，筋特異的microRNA（*miR-1, 133a, 133b, 206*）が，他の小児がん細胞株に比べて高発現していることが報告されている[37,38]．一方，血清中に腫瘍由来のmiRNAが存在することも明らかにされ，大腸がん，リンパ腫，前立腺がん，肝がんなどで，miRNAのバイオマーカーとしての有用性が示唆されている[39-42]．これらの血清中の遊離microRNAは多量に，比較的安定して存在しており，バイオマーカーとして期待されている[40]．そこで，我々は，筋特異的microRNAが横紋筋肉腫患児の血清診断に応用可能ではないかと考え検討を行った．

横紋筋肉腫8例，非横紋筋肉腫23例を対象として，血清200 μLを用いてmicroRNAを抽出し，定量的リアルタイムPCRにより定量を行った[43]．群間比較はMann-Whiteny U検定を，診断精度の指標としてROC曲線を用いて解析を行った．血清中の筋特異的microRNA（miR-1，133a，133b，206）の発現は，非横紋筋肉腫症例に比して，横紋筋肉腫症例において有意に増加していた（$p<0.05$）．とくに，*miR-206*については，感度1.0，特異度0.913と診断的バイオマーカーとして有用であることが分かった．また，血清*miR-206*上昇症例においては，治療が奏功した場合，血清*miR-206*の低下を認めた．以上より，筋特異的microRNAである*miR-206*が横紋筋肉腫患児の血清診断に応用可能であることを示した．

さらに症例数を増やした横紋筋肉腫21例，非横紋筋肉腫28例の解析では，感度0.809，特異度0.893であり，血清*miR-206*が上昇している場合，高い精度で横紋筋肉腫であることを示すことが分かった．さらに，領域リンパ節転移（N1），遠隔転移（M1）症例の*miR-206*発現は，これらを有さない（N0，M0）症例と比して，有意に上昇していた（$p=0.01$）[44]．

以上より，横紋筋肉腫診療において，血清*miR-206*発現の定量は，診断，治療反応性のモニタリングに有用であることが分かった．また，*miR-206*の高発現は，転移症例と相関しており，高発現と予後不良との相関が予想される．JRSGの次期臨床試験JRS-IIでは全リスク群プロトコルで診断時，治療経過中の血清*miR-206*の定量を行う予定であり，診断のみならず，予後との相関についても検証する予定である．

VIII　おわりに

米国とわが国の横紋筋肉腫治療研究の現況と今後の展望について概説した．また，可能性のある新規バイオマーカーについても言及した．強化療法で治療成績の向上した低リスク群や中間リスク群では治療減量・期間や新規薬剤導入による晩期合併症の軽減化が図られており，治療成績の改善のない高リスク群では新たな治療法が模索されている．AYA世代では一般に低リスク群も含め，小児より治療成績が悪い傾向があり，今後はこれらの年齢層も含めた多施設共同臨床研究が必要であろう．

謝　辞

有益な討議の機会と貴重な情報提供をいただいたChildren Oncology Group Soft Tissue Sarcoma Study Committee（COG-STS）のDougrous Hawkins委員長，新規薬剤について情報を提供していただいた同Peter Houghton博士，日本